Sensors and Materials, Vol. 35, No. 12 (2023) 4141–4166
MYU Tokyo

S & M 3473

Next-generation Electrochemical Sensors for Detection of Respiratory Viruses

Atakan Akdag,[1] Dilan Seyman,[1] Charles S. Henry,[2,3] Osman Sagdic,[4] Atchara Lomae,[3] Nipapan Ruecha,[3,5] Tirayut Vilaivan,[6] Orawon Chailapakul,[5*] and Tugba Ozer[1,7**]

[1]Yildiz Technical University, Department of Bioengineering, Faculty of Chemical-Metallurgical Engineering, Istanbul 34220, Türkiye
[2]Colorado State University, School of Biomedical Engineering, Department of Chemistry, Fort Collins, Colorado 80523, USA
[3]Chulalongkorn University, Metallurgy and Materials Science Research Institute, Bangkok 10330, Thailand
[4]Yildiz Technical University, Department of Food Engineering, Faculty of Chemical-Metallurgical Engineering, Istanbul, Türkiye
[5]Chulalongkorn University, Electrochemistry and Optical Spectroscopy Center of Excellence (EOSCE), Department of Chemistry, Faculty of Science, Bangkok 10330, Thailand
[6]Chulalongkorn University, Organic Synthesis Research Unit, Department of Chemistry, Faculty of Science, Bangkok 10330, Thailand
[7]Yildiz Technical University, Health Biotechnology Joint Research and Application Center of Excellence, 34220 Esenler, Istanbul, Türkiye

(Received April 26, 2023; accepted July 5, 2023)

Keywords: electrochemical biosensor, respiratory virus, airborne, point-of-care, COVID-19

Respiratory viruses have caused many deaths, severe cases, epidemics, and pandemics. Therefore, reliable, rapid, selective, and sensitive detection and quantification of respiratory viruses are necessary to prevent the spread of transmission and future pandemics. Recently, studies on the detection of respiratory viruses have focused on electrochemical biosensors, especially for coronavirus disease 2019 (COVID-19), owing to their advantages such as low cost, fast response, and point-of-care applications. In this review, recent developments and applications of antibody-based, nucleic-acid-based, and aptamer-based biosensors for the electrochemical sensing of respiratory viruses from the years 2021 to 2023 are presented. Modification concepts and working principles of these biosensors are also demonstrated. In addition, the advantages and challenges of each biosensor and future prospects are discussed.

1. Introduction

Respiratory viruses, including avian influenza, rhinovirus, adenovirus, severe acute respiratory syndrome coronavirus 2 (SARS-CoV-2), severe acute respiratory syndrome coronavirus 1 (SARS-CoV-1), Middle East respiratory syndrome 2 (MERS-CoV-2), and respiratory syncytial virus (RSV), endanger human health and cause common symptoms such as sputum, dry cough, loss of smell, fatigue, and fever in patients upon exposure to aerosolized

*Corresponding author: e-mail: corawon@chula.ac.th
**Corresponding author: e-mail: tozer@yildiz.edu.tr
https://doi.org/10.18494/SAM4469

ISSN 0914-4935
https://myukk.org/

virus particles and contact with contaminated surfaces.[1–8] Diseases caused by respiratory tract viruses have caused severe cases and pandemics.[3,5] For example, RSV causes 14,000 deaths in people over 65 years of age in the United States annually.[9] Moreover, the influenza virus has been identified as the most common infectious disease and has resulted in three pandemics in the 20th century.[10] In 2019, the COVID-19 pandemic led to many deaths and economic loss worldwide, showing the importance of preparedness for pandemics.[11]According to the World Health Organization (WHO), there were over 760 million cases and six million deaths worldwide as of 01 April 2023.[12] Owing to the rapid transmission from positive asymptomatic individuals, early detection of SARS-CoV-2 and then isolation of infected patients are crucial to prevent a pandemic.[13]

Viruses can be categorized in accordance with their phenotypic characteristics, which include their morphology, genome structure, mechanism of replication, and shape.[14] Depending on the presence of an envelope, viruses are classified as enveloped and nonenveloped viruses. MERS, swine flu, SARS-CoV-2, influenza, and RSV are enveloped viruses.[15,16] Among them, the coronavirus family, having a spherical shape with a diameter of 60–220 nm, contains single-stranded ribonucleic acid (RNA) and nucleocapsids containing spike (S), envelope (E), membrane (M), and nucleocapsid (N) proteins.[17, 18] These proteins can be used as targets for the detection of SARS-CoV-2. The S protein shows high immunogenicity and is found in the transmembrane, whereas the N protein is responsible for the viral replication cycle.[19] Since S and N proteins are highly specific to SARS-CoV-2, they are mostly preferred as biomarkers.

The receptor binding domain (RBD) is also used as a target region owing to the presence of their s1 subunit specific to the angiotensin-converting enzyme II receptor in human cells.[20] Although open reading frame 1a (ORF1a)/b genes encoding S and N proteins are used as targets in the detection of SARS-CoV-2, there is a 79% similarity between SARS-CoV and SARS-CoV-2 genomes. Therefore, more specific primers for SARS-CoV-2 should be identified.[20, 21] In addition, immunoglobulin G (IgG), immunoglobulin M (IgM), and immunoglobulin A (IgA) antibodies can be used as targets.[22]

Influenza virus subunits include strains A, B, and C consisting of matrix protein 1 (M1), hemagglutinin (HA), and neuraminidase (NA) surface proteins as biomarkers.[23] Similarly, the S protein is more widely used than other surface proteins as an antigen for MERS-CoV detection since it directly binds to the host cell.[24] There are 11 ORFs and 30119 nucleotides in the MERS-CoV genome. Genes located downstream of ORFs 1a and 1b in the 50-translated region (UTR) encode structural proteins.[25] For MERS-CoV RNA-based detection, the WHO promotes the use of the E gene region as a target, whereas the FDA promotes the use of the N gene for the detection of MERS-CoV.[26, 27]

Although infected people can produce antibodies in response to MERS-CoV antigens, such as S, 3a, N, and 9b, MERS-CoV antigens are not suitable for the early diagnosis of the disease. However, MERS-CoV antigens can be used for the detection of respiratory viruses in patients during the recovery period.[28] There are 10 genes in the RSV genome, which encode 11 different proteins.[3] They are subdivided into A and B subgroups in accordance with variants in the RSV genome sequence and the reactivity of antibodies to surface glycoprotein (G) and fusion protein (F).[29,30] F and G proteins can be targeted directly, as well as gene sequences encoding F and G proteins for the detection of the RSV virus.[3]

The majority of traditional procedures for detecting respiratory viruses are lab-based methods.[24] The real-time reverse transcription-polymerase chain reaction (RT-PCR) technique is one of the laboratory techniques used for respiratory virus detection.[31] However, trained personnel are necessary to implement this technique, and the time required for gene amplification can be up to 4 h .[31] Owing to its high cost and requirement of multiple steps to prepare the sample, this technique is not suitable for large-scale sample monitoring and point-of-care (POC) testing.[32] Another traditional method used for virus detection is the enzyme-linked immunosorbent assay (ELISA).[33] ELISA can identify and measure human IgG, IgM, or total IgGs from the serum or plasma sample.[34] However, the tests used to detect these antibodies have low sensitivity and specificity.[35] The immunofluorescence assay, isothermal amplification techniques, and immunochromatography have also been used as traditional methods.[24] Although these techniques offer high sensitivity, they are time-consuming and costly and require qualified personnel to perform.[36]

The rapid detection of pathogens that cause respiratory infections is crucial to control the spread of the disease and to prevent infections.[37] Electrochemical biosensors have attracted considerable interest owing to their low cost and rapid response in the detection of viruses.[36] In addition, the sensitivity of the sensor can be improved with the use of nanomaterials developed by different strategies.[38] It is also possible to create miniaturized components on a single platform by combining electrochemical biosensors with microfluidic systems using a small volume of sample.[36]

In this review, recent developments and applications of electrochemical biosensors for the sensing of respiratory viruses from 2021 to 2023 are presented. Recent reports on the electrochemical biosensor have mainly been focused on the SARS-CoV-2 virus in the last two years owing to the COVID-19 pandemic (Table 1 in Sect. 4). Future prospects are discussed in the conclusions section.

2. Antibody-based Electrochemical Biosensors

Antigens or antibodies as biorecognition elements are used for the development of immunosensors. Antibodies, which are serum proteins produced by antigen reorganization cells such as B-lymphocytes and plasma cells, are specific to antigens. Antibodies are used as biorecognition elements in biosensors owing to their high specificity and affinity.[24,39] Antibody single-chain variable fragments (scFvs), polyclonal antibodies (pAbs), and monoclonal antibodies (mAbs) are generally used to detect respiratory viruses.[40] While mAbs are capable of reacting with a single epitope, pAbs can react with multiple epitopes on an antigen.[41] As a result, mAbs are more specific than pAbs, and the use of mAbs in immunosensors decreases cross-reactivity with other viruses.[42] On the other hand, pAbs reduce immunosensor cost since the production of pAbs is less expensive and requires less time than that of mAbs.[43] scFvs are ~30 kDa, consist of a light chain and a heavy chain, and are also used as recognition elements.[44] scFvs display less variability and are smaller than native antibodies; however, they require more pretreatment to be used as a biorecognition element.[45]

Drobysh *et al.* reported an immunosensor to detect SARS-CoV-2 in blood serum.[46] A gold (Au) electrode was activated by dipping into an 11-mercaptoundecanoic acid solution. SARS-CoV-2 spike protein (rspike) was immobilized on the Au electrode by using 1-ethyl-3-(3-dimethylaminopropyl)-carbodiimide/N-hydroxysuccinimide (EDC/NHS) chemistry. With a platinum (Pt) counter electrode and silver/silver chloride (Ag/AgCl) as the reference electrode, cyclic voltammetry (CV) and electrical impedance spectroscopy (EIS) were used to detect SARS-CoV-2-specific antibody in blood sera collected from COVID-19 patients. The limits of detection (LODs) were found to be 2.53 and 1.99 nM using CV and EIS, respectively. However, the biosensor was not validated against conventional methods. In another report, Ashur *et al.* reported a biochip modified with anti-spike mAbs (S-abs) to detect SARS-CoV-2 spike protein.[47] A Au electrode was fabricated via the lift-off method on a p-doped silicon/silicon oxide (Si/SiO_2) substrate. Then, S-ab was covalently immobilized to the surface of the Au electrode via the thiol modification of primary amines by incubation with 2-iminothiolane (2-IT; Traut's reagent) for 1 h. SARS-CoV-2 pseudovirus particles, which are virus-like particles, were used as samples to investigate the sensitivity of the biosensor. Vesicular stomatitis virus (VSV) was used to synthesize SARS-CoV-2 pseudovirus particles including the spike S1 protein (S1) and RBD of the SARS-CoV-2 spike protein. SARS-CoV-2 pseudovirus in phosphate-buffered saline (PBS) was drop-cast on the electrode surface. The electrochemical measurements were carried out using EIS. The LOD was determined as 1.1×10^5 gcn mL^{-1} (gene copy number per milliliter) within the linear range of 10^4–10^9 virus particles mL^{-1}. The analysis time was determined as 30 min.

Similarly, Kowalczyk *et al.* reported an electrochemical biosensor for the detection of SARS-CoV-2 spike protein.[48] A Au electrode was activated using cysteamine hydrochloride (CSH) to immobilize recombinant SARS-CoV-2 monoclonal antibodies with EDC/NHS chemistry. N-(4-aminophenyl)ferrocenecarboxamide was synthesized as described in a previous report.[49] Fc-R-COOH redox probes were produced and diluted with methylene chloride. Secondary commercial recombinant SARS-CoV-2 monoclonal antibodies were immobilized to the Fc-R-COOH surface with the use of EDC/NHS chemistry. To perform the electrochemical measurements in the presence of Pt and Ag/AgCl electrode as the counter and reference electrodes, respectively, the sample was introduced to the antibody-modified electrode surface. Then, a secondary antibody–Fc-R-COOH complex was added to the electrode surface to generate a sandwich form. Nasopharyngeal swabs obtained from patients were used to detect SARS-CoV-2 S protein via differential pulse voltammetry (DPV). The linear range of detection was 0.2–2.10×10^5 pg ml^{-1} whereas the LOD was 0.08 pg ml^{-1}. The biosensor was validated by PCR using clinical swabs and saliva samples with an average accuracy of 92.8%. In addition, the immunosensor was found to be stable for 30 days. Zargartalebi *et al.* reported an electrochemical immune based biosensor that can detect nucleoproteins and viral particles of SARS-CoV-2.[50] An Au electrode was modified with SARS-CoV-2 antibody. Two conjugated DNA probes (P1 and P2) were used to immobilize the antibodies on the electrode surface. The thiolate probe 1 (P1) solution was mixed with tris(2-carboxyethyl) phosphine hydrochloride (TCEP) solution. After that, antibody-conjugated probe 2 (P2) and 6-mercapto-1-hexanol (MCH) were added to the P1-P2-antibody

solution. The final solution was incubated on the electrode surface for 4 h. Then, electrochemical measurements were carried out by chronoamperometry (CA). While the linear range of detection was 0.01–10000 pg mL^{-1}, the LOD was 1 fg mL^{-1} for SARS-CoV-2 nucleoproteins. Moreover, SARS-CoV-2 from patients' clinical saliva samples was detected and the LOD was found to be 20 copies mL^{-1} for SARS-CoV-2 viral particles within the linear range of 10^3–10^7 copies mL^{-1}. The results were validated by real-time PCR with an accuracy of 93%.

In the last decade, paper-based analytical devices (PADs) have attracted attention owing to their unique properties such as low cost, disposability, environmental friendliness, and ease of fabrication. For example, Yakoh *et al.* developed a label-free paper-based electrochemical device (ePAD) to diagnose COVID-19.[51] Three electrodes, namely, working, counter, and reference electrodes, were screen-printed on a paper substrate, limiting the hydrophilic zones of each layer by a wax barrier to let the analyte flow into the testing area. After a commercial graphene oxide (GO) solution was drop-cast on the working electrode, SARS-CoV-2 antibodies (both IgG and IgM) were immobilized via EDC/NHS chemistry. Skim milk was used as a blocking agent to prevent nonspecific binding. The sensing was based on the immunocomplex between the spike protein of SARS-CoV-2 and immunoglobulins in the human response to SARS-CoV-2 using square wave voltammetry (SWV). The LOD was found to be 1 ng mL^{-1}. The ePAD was applied to 17 actual serum samples, seven of which had SARS-CoV-2, and showed high sensitivity (100%) with an analysis time of ~ 30 min. Another PAD was reported by Pola *et al.* to detect the SARS-CoV-2 spike RBD.[52] The electrode was fabricated using graphene ink via aerosol jet printing. Then, SARS-CoV-2 spike rabbit polyclonal antibodies were immobilized to the electrode surfaces through carbodiimide bonds using EDC/NHS crosslinkers. EIS was used to detect whole spike protein in 33 min. The linear range was found to be 1–1000 ng ml^{-1} with an LOD of 110.38 ± 9.00 pg ml^{-1}. The selectivity test of the developed immunosensor was performed, and no crosstalk with other respiratory viruses, including MERS-CoV and influenza H1N1 viruses, was found.

Zamzami *et al.* reported an electrochemical biosensor for the detection of SARS-CoV-2 spike protein (S1) from saliva samples.[53] The electrode consists of three parts: source, gate, and drain. Ti 10 nm/Au 30 nm were used to fabricate the source and drain (S–D) parts of the electrode by photolithography and lift-off techniques. A commercial carbon nanotube (CNT) was mixed with 1,2-dichlorobenzene and centrifuged to remove aggregates. The CNT suspension was loaded on an injection printer and printed onto a Si/SiO_2 substrate of the electrode gate part. Monoclonal anti-SARS-CoV-2 S1 antibodies were immobilized using 1-pyrene butanoic acid succinimidyl ester (PBASE) as a crosslinker to the CNT-modified electrode surface. The SARS-CoV-2 S1 spiked in saliva samples was detected by using source-drain currents (IDS), and the LOD was found to be 4.12 fg mL^{-1} within the linear range from 0.1 fg mL^{-1} to 5.0 pg mL^{-1}. The selectivity of the biosensor was investigated using a mixture of SARS-CoV-2 S1, SARS-CoV-1 S1, and MERS-CoV S1 in ammonium acetate buffer solution, and the biosensor showed no crosstalk with other respiratory viruses. The reproducibility of the biosensor was confirmed via 24 consecutive measurements. However, the sensitivity of the developed biosensor should be investigated in actual samples.

Clark *et al.* reported an electrochemical capillary-driven immunoassay (eCaDI) to detect SARS-CoV-2 nucleocapsid (N) protein [Fig. 1(A)].[54] Capillaries of the device were generated using a CO_2 laser on a polyethylene terephthalate (PET) film, whereas the electrodes were screen-printed on a PET film using carbon ink. The screen-printed electrode (SPE) surface was modified with commercial SARS-CoV-2 anti-N antibodies via drop-casting. The detection was based on a sandwich-type immunoassay by incubating 3,3′,5,5′-tetramethylbenzidine (TMB) reagent and horseradish peroxidase (HRP)-antibody conjugate solution on conjugate pads placed in the capillaries of the device. Once the N protein in the sample was captured by the antibody immobilized on the electrode surface, the HRP-antibody conjugate and TMB reagent reach the electrode surface via the flow in the capillaries. After the sandwich-type immunoassay was completed, chronoamperometry was used to detect the N protein. The linear range of N protein detection was determined as 5 to 106 equivalent PFU mL^{-1}, whereas the LOD was determined as 68 equiv PFU mL^{-1}. The analysis time was determined as 25 min, which is less than the time required to perform ELISA. In addition, it offers automated steps, enabling its use by an untrained end-user. The eCaDI has advantages, namely, it remains stable for 24 days and is able to detect different variants of SARS-CoV-2 with no cross-reactivity with influenza and Sindbis viruses. However, the sensitivity of the eCaDI should be investigated in clinical samples.

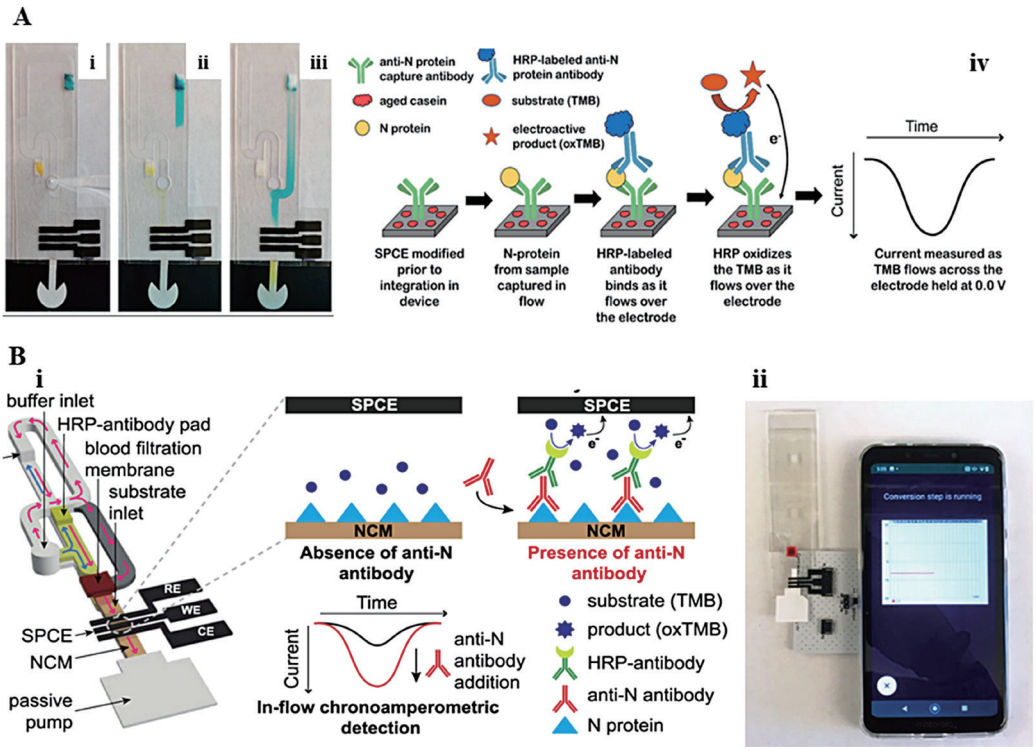

Fig. 1. (Color online) (A) (i) Schematic representation of layers of eCaDI. (ii) Sample loading and then delivery of HRP-antibodies (with yellow dye). (iii) Delivery of TMB (with blue dye) to the SPCE by the flow of the eCaD. Adapted with permission from Ref. 54 (Copyright 2022, American Chemical Society). (B) Schematic representation of (i) detection mechanism and automatic formation of immunoassay and (ii) smartphone-based detection system connected to the NFC potentiostat for POC application. Adapted with permission from Ref. 55 (Copyright 2021, American Chemical Society).

The same group reported an electrochemical capillary-flow device that detects IgG antibodies produced against SARS-CoV-2 N proteins in human blood samples [Fig. 1(B)].[55] The electrochemical capillary-flow device was developed to enable automatic ELISA. The device consists of two parts, namely, stacked layers of hydrophilic polyester and double-sided adhesive films. A screen-printed carbon electrode (SPCE) was fabricated using carbon ink and a polyester film. The capillaries of the device were generated using a CO_2 laser, and a filter was placed where the sample was introduced to eliminate impurities in the blood. An HRP-antibody pad and a functionalized nitrocellulose membrane (NCM) with recombinant N protein were used to perform immunoassay on capillary tubes. The HRP-antibody solution was prepared using ferrous sulfate-edetic acid ($FeSO_4$-EDTA), trehalose, and bovine serum albumin (BSA), followed by addition on the glass fiber pads. A solution of recombinant N protein was prepared in trehalose and glycerol, and then striped on the commercial NCM using a reagent dispenser. A recombinant N protein-modified HRP-antibody reagent pad and NCM were placed inside the channels. Anti-N antibodies were captured by the nucleocapsid protein from the membrane, and then HRP-labeled antibodies were captured by anti-N antibodies. Finally, the TMB solution was drop-cast on the NCM membrane. An SPCE was also placed on the NCM, and a commercial smartphone-based near-field communication (NFC) potentiostat was connected to carry out chronoamperometry. The linear range was obtained as 0–100 ng mL^{-1}, whereas the LOD was determined as 5 ng mL^{-1}. The analysis time was 20 min. The developed biosensor can detect SARS-CoV-2 at the POC.

Lee *et al.* reported a paper-based label-free immunosensor to detect H5N1, H7N9, and H9N2 avian influenza viruses.[56] The electrodes were screen-printed using a mixture of multiwalled carbon nanotubes (MWCNTs) and polydimethylsiloxane (PDMS) on a paper substrate. Antibodies specific to the HA proteins of H5N1, H7N9, and H9N2 were individually immobilized to the SPE surface using EDC/NHS chemistry. DPV was used to perform electrochemical measurements, and the LODs were found to be 55.7, 99.6, and 4.0 pg mL^{-1} for H5N1, H7N9, and H9N2 HA, respectively. Although it is possible to simultaneously detect avian influenza viruses including H5N1, H7N9, and H9N2, the selectivity of the sensors should be evaluated to show the applicability of the developed biosensor in the real world. Recently, nanofibers consisting of cellulose, carbon nanotubes, and carbon nanofibers (CNFs) have become popular for the construction of biosensors to facilitate electrolyte penetration owing to their porous nature. Eissa *et al.* reported a CNF-based sensor for the detection of MERS-CoV.[57] Carbon electrodes were screen-printed and modified with commercial CNF. Then, MERS-CoV spike protein antibodies were immobilized via EDC/NHS chemistry. SWV was used to detect MERS-CoV spike protein and the LOD obtained was determined as 0.07 pg·mL^{-1} within the linear range from 0.1 pg·mL^{-1} to 1 μg·mL^{-1}. A smartphone-based potentiostat was used to carry out SWV. Spiked nasal samples were analyzed using the developed biosensor and the recoveries were determined to be between 91.5 and 96%. The biosensor remained stable for seven days.

Recently, magnetic beads (MBs) have become popular owing to their compatibility with antibodies and fewer washing and separation steps. Fabiani *et al.* reported an immunoassay-based biosensor to detect the spike and nucleocapsid proteins of SARS-CoV-2 in untreated saliva samples.[58] The electrode was fabricated via screen-printing using graphene ink and carbon

black. Mouse IgG was drop-cast on the electrode surface for functionalization. Then, MBs were incubated with BSA as a blocking agent for 30 min at room temperature. Monoclonal anti-SARS-CoV-2 antibodies were coated on MBs. Polyclonal anti-SARS-CoV-2 antibodies and polyclonal antibodies labeled with alkaline phosphatase anti-rabbit IgG in PBS were mixed with a blocked MB suspension for 30 min. The suspension was prepared in diethanolamine buffer and then drop-cast onto the modified SPE surface. Then, a magnet was placed under the SPE. After 1-naphthyl phosphate was incubated on the electrode surface for 2 min, 1-naphthol as the enzymatic product was detected using DPV. The applicability of the electrochemical immunoassay was tested using the standard solution of S and N protein targets in buffer and saliva samples, and the LODs were found to be 19 and 8 ng mL^{-1}, respectively. The selectivity of the biosensor was evaluated towards influenza H1N1 virus and no crosstalk was found. The advantage of this biosensor is that no pretreatment was applied to the saliva samples before use. Another MB-assisted immunosensor to detect SARS-CoV-2 spike protein (S1) spiked in PBS and nasopharyngeal samples was developed by Zhao *et al.* [59] A glassy carbon electrode (GCE) was used as the working electrode and modified to immobilize spike antibodies. At first, a palladium–gold (Pd–Au) nanosheet was synthesized in the presence of palladium(II) 2,4-pentanedionate (Pd(acac)2) in glacial acetic acid and CO gas for 30 min. The Pd nanosheet was then ultrasonically thawed to obtain a Pd–Au composite nanosheet. $HAuCl_4{\cdot}3H_2O$ was added dropwise to the solution and mixed for 1 h to generate a Pd–Au nanosheet. The Pd–Au nanosheet solution was drop-cast on the GCE surface. Sulfhydryl groups of S1 antibodies were generated using UV light of 300 mW cm^{-2} for 30 s and immobilized on a PdF–Au modified electrode. BSA was used to prevent nonspecific adsorption on the electrode surface. Antibody-modified magnetic nanoparticles (MNPs) were prepared and added to the spike sample solution. The MNPs–antibody-spike protein (MNPs-ab-S1) complex solution was drop-cast on the GCE surface and used to detect SARS-CoV-2 using DPV in the presence of a saturated calomel electrode as the reference electrode and a Pt electrode as the counter electrode. The linear range of detection was from 0.01 to 1000 ng mL^{-1} with an LOD of 0.0072 ng mL^{-1} in spiked PBS with an analysis time of 2 h. The biosensor was validated in spiked nasopharyngeal samples with recoveries between 84.545 and 103.520%. Another MNP-based biosensor was reported for the detection of SARS-CoV-2 by Durmus *et al.*[60] MNPs were synthesized in accordance with the protocol of Sanli *et al.*[61] The surface of the MNPs was activated using tetraethyl orthosilicate, and then EDC/NHS coupling was used to immobilize SARS-CoV-2 spike 1 (S1) and spike 2 (S2) proteins. MNP–antibody conjugations including variants of SARS-CoV-2 were also prepared. An antigen–MP complex was drop-cast and immobilized to the SPE surface with the use of a magnet placed on the back of the electrode. Finally, an antibody–MNP suspension was added, and electrochemical measurements were performed using DPV. The LODs were found to be 0.53 and 0.75 ng mL^{-1} within the linear ranges of 1.0–200 ng mL^{-1} and 2.5–100 ng mL^{-1} for purified S1/Ab and S2/Ab, respectively. The results were confirmed by PCR in clinical nasopharyngeal samples with 100% accuracy.

Plant-based systems to produce mAbs have attracted attention owing to their low-cost, high-scale manufacturing and low risk of pathogen contamination in humans.[62] Since mammalian cells might include pathogens, plants are preferred to produce antibodies owing to the lack of

contamination risks. Jaewjaroenwattana *et al.* developed a paper-based electrochemical sensor modified with plant-derived mAb CR3022 for detecting SARS-CoV-2 antigen.(63) While the working and counter electrodes were fabricated using graphene ink, the reference electrode was generated using Ag/AgCl ink via screen-printing. Then, commercial cellulose nanocrystal (CNC) water was incubated on an SPE via drop-casting for 15 min, and antibodies were immobilized owing to the presence of COOH groups on the electrode surface via EDC-NHS coupling for 1 h. After that, skim milk was used as the blocking agent to prevent nonspecific protein binding. The RBD spike protein of SARS-CoV-2 was detected using DPV, and the LOD was found to be 2.0 fg mL^{-1} in the linear range from 0.1 pg mL^{-1} to 500 ng mL^{-1}. The biosensor was tested in artificial saliva samples spiked with RBD and recoveries were found to be between 0.6 and 13.2%.

There is also growing interest in developing molecularly imprinted polymers (MIPs), which are synthetic polymer matrices with specific molecular recognition sites to distinguish molecules.(64) MIPs are suitable alternatives to antibodies owing to their enhanced chemical and thermal stabilities, reproducibility, and low cost. Ayankojo *et al.* reported an MIP-based electrochemical sensor [SARS-CoV-2 spike protein subunit S1 (ncovS1)-MIB] that detects SARS-CoV-2 spike protein.(64) A commercial Au-thin-film metal electrode (Au-TFME) as the working electrode was incubated with 4-aminothiophenol (4-ATP) in ethanol and 3,3′-dithiobis (sulfosuccinimidyl propionate).Then, the ncovS1 antigen was immobilized to a modified electrode, followed by the synthesis of poly (3-aminophenyl boronic acid) (PAPBA) to generate MIP for the specific detection of spike protein owing to the formation of covalent bonds between the target and the monomer. After the synthesis of PAPBA, disulfide bonds were cleaved and spike proteins were removed from the electrode surface. SWV was applied and the linear range was between 0 and 400 fM with an LOD of 65 fM in clinical samples. The detection time was determined as 15 min. The developed biosensor enables the rapid detection of SARS-CoV-2 in actual samples; however, its cross-reactivity with other respiratory tracts should be evaluated.

Perdomo *et al.* developed a portable biosensor named SenSARS for the detection of SARS-CoV-2.(65) With the use of a planar three-electrode electrochemical cell configuration, the electrodes were fabricated on a PET film by screen-printing. The surface of the SPE was modified using para-aminobenzoic acid (PABA) by electrodeposition. EDC/NHS was used to immobilize mAb on the modified electrode surface owing to the presence of the carboxyl end of PABA. Then, BSA was used as a blocking agent. The LOD was determined as 1.065 fg mL^{-1} using EIS. The selectivity of the biosensor was investigated using SARS-CoV-2 (S), Epstein–Barr virus (EBV) glycoprotein gp350, and influenza H1N1 recombinant viral proteins in PBS, and no crosstalk was observed. The SenSARS provides a potential route for fast (~10 min) COVID-19 diagnosis. Sharma *et al.* reported an immunosensor for the detection of SARS-CoV-2 spike protein.(66) A platinum–titanium (Pt/Ti) electrode double-interdigitated capacitive (DIDC) chip as the working electrode was activated using piranha solution and coated with graphene oxide (GrO) via spin coating. Then, EDC/NHS were used to immobilize SARS-CoV-2 Abs produced using the rabbit mAbs anti-S1 protein. SARS-CoV-2 spike protein was detected in PBS by the capacitance measurement. The linear range was determined as 1.0 mg mL^{-1}–1.0 fg mL^{-1} with a LOD of 1 fg mL^{-1}, and the detection time was 3 s. The stability of the biosensor was 10 days.

Chen *et al.* reported an electrical-double-layer gated field-effect transistor-based biosensor (BioFET) to detect the SARS-CoV-2 nucleocapsid protein.[67] Eight electrodes were modified with SARS-CoV-2 N protein antibodies using Traut's reagent via thiolated primary amine groups of the anti-N antibodies. The linear range of the SARS-CoV-2 N detection was found to be from 0.4 to 400 ng mL^{-1} with LODs of 7.44 and 2.96 pM in PBS and artificial saliva samples, respectively, using SWV via a commercial smartphone-based potentiostat. The detection time was determined as 30 min. However, reproducibility and stability tests should be carried out. Also, the biosensor should be validated in real clinical samples. Li *et al.* reported a multichannel electrochemical immunosensor for the simultaneous detection of the viruses SARS-CoV-2 and influenza A (H1N1) in human serum samples.[68] Commercial SPCEs were used to immobilize influenza A (H1N1)/BJ501 antibodies, and SARS-CoV-2 spike antibodies were immobilized via drop-casting. Influenza A (H1N1)/BJ501 or SARS-CoV-2 spike protein was drop-cast, followed by incubation with HRP-labeled SARS-CoV-2 and influenza A (H1N1)/BJ501 antibodies. Finally, 3,3',5,5'-tetramethylbenzidine (TMB) solution was incubated on SPEs. While the linear range was determined as 4–64 units mL^{-1} with an LOD of 1.12 U mL^{-1} for influenza A (H1N1), the linear range was determined as 0.15–100 ng mL^{-1} with an LOD of 0.15 ng mL^{-1} for SARS-CoV-2 using amperometry. The total analysis time was 2 h. It was possible to simultaneously detect influenza H1N1 and SARS-CoV-2 with an accuracy of 94.6% compared with ELISA. Also, recoveries were determined as 95–100%.

In recent years, 3D printing technology has attracted for the fabrication of electrodes owing to the ease of mass production of a customized shapes.[69] Polylactic acid (PLA) is commonly used as the conductive polymer owing to its biocompatibility and low temperature for printing. Stefano *et al.* reported an immunosensor for the detection of SARS-CoV-2 spike protein.[70] 3D-printed electrodes were fabricated using graphite and PLA. After graphite was dispersed in a mixture of ethanol and chloroform, PLA was added to the solution to form GPT/PLA filaments via recrystallization. Then, the GPT/PLA filaments were used as the substrate to fabricate 3D-printed electrodes, and SARS-CoV-2 spike antibodies (S1Ab) were immobilized via EDC/NHS chemistry. BSA was added to the electrode surface to prevent nonspecific interactions. The LOD was 1.36 nM within a linear range of 5.0–75.0 nM using CV. Artificial saliva samples in PBS were tested using the developed biosensor with recoveries between 86.3 ± 2.7% and 96.1 ± 10.2%.

Artificial intelligence and machine learning (ML) have been rapidly adopted owing to their ability to deal with high-throughput data.[71] ML algorithms can solve problems such as electrode fouling, poor signal-to-noise ratio, and chemical interferences by evaluating big data. Fortunati *et al.* reported a portable biosensor enhanced with ML for the detection of SARS-CoV-2 spike protein.[72] An SPE was modified with AuNPs, and SARS-CoV-2 monoclonal S1 antibodies (S1-Abs) were immobilized via drop-casting. The spike protein detection capacity of the biosensor was tested using a commercial SARS-CoV-S1 protein in tris(hydroxymethyl)aminomethane (TRIS) solution mixed with polyclonal anti-spike protein and goat anti-rabbit IgG secondary antibody conjugated with alkaline phosphatase (GAR-AP). The final solution was incubated on S1-Ab-modified electrodes via drop-casting. Finally, hydroquinone diphosphate (HQDP) was added to the electrode surface to react with GAR-AP. DPV was used for spike protein detection

and the LOD was found to be 12 ng mL^{-1} within the linear range of 0.5–5 μg mL^{-1}. For SARS-CoV-2 spike protein samples, the linear range of detection was determined as 6.3×10^7 to 1.9×10^6 transducing units (TU) mL^{-1}. Also, the accuracy of the biosensor was investigated with a collection of 108 data, namely, 55 positive and 53 negative clinical samples, and was found to be 97.3%. The analysis time was 1 h. The developed biosensor has the disadvantage that the samples should be pretreated before use.

In another study, Witt *et al.* reported a boron-doped diamond (BDD) impedimetric biosensor for the detection of SARS-CoV-2 spike (S1) protein.[73] BDD films were generated in three different thicknesses to investigate the effect of the thickness on the detection. Thicknesses of 3.6 and 0.7 μm were generated via the microwave plasma-assisted chemical vapor deposition (MWPA-CVD) method, whereas a thickness of 8 μm was generated by the hot filament chemical vapor deposition (HF-CVD) method. The OH groups on BDD films were activated with the use of (3-aminopropyl) trimethoxysilane, followed by the incubation of EDC/NHS to immobilize the spike S1 antibody. The LOD was determined as 1 fg mL^{-1} by using EIS. The applicability of the biosensor should be evaluated in clinical samples.

2D transition metal carbide and nitride (MXene) have become popular among post-graphene materials used in biosensor development owing to their properties such as enhanced catalysis and conductivity. [74]A transition metal, including Ti, Mo, or Nb, exists in their structure, whereas X represents carbon or nitrogen content. Lin *et al.* reported a pH-sensitive sandwich-type biosensor based on a titanium carbide (Ti_3C_2)–MXene nanosheet to detect the influenza H1N1 virus.[75] A sandwich-type immunoassay was generated by modifying a commercial microplate and Ti_3C_2–MXene nanosheets. At first, the microplate was coated with monoclonal antibodies. Then, Ti_3C_2–MXene nanosheets were synthesized by the HF-etching batch Ti_3AlC_2 method and functionalized by coating with polyclonal antibodies.[76] The modification of Ti_3C_2–MXnene nanosheets with glucose oxidase (Gox) and pAB2 was achieved via epoxy-amino reaction. Ti_3C_2–MXnene nanosheets were added to the (3 glycidyloxypropyl)trimethoxysilane (GOPS) solution to form epoxy groups (such as -OH groups) on the surface of Ti_3C_2–MXnene nanosheets. Then, GOx and pAB2 were dissolved in PBS, and the solution was mixed overnight with the activated Ti_3C_2–MXnene nanosheets. Thus, the modification of the Ti_3C_2–MXene nanosheets was completed and GOx–Ti_3C_2–pAb2 was formed. After that, GOx–Ti_3C_2–pAb2 was injected into microplate wells and then glucose was added. Gluconic acid was formed by the reaction between glucose and glucose oxidase, causing changes in the pH. The pH change was measured using a commercial pH electrode. The calibration curve was determined owing to the linear correlation between the logarithms of the influenza H1N1 concentration and the pH values. The linear range of detection was determined as 0.01–100 μg mL^{-1}, whereas the LOD was determined as 1.3 ng mL^{-1}. The optimal time for immunoreaction was determined as 50 min. The stability of the developed pH-sensitive sandwich-type immunoassay should be investigated owing to the instability issues with enzymes.

Takemura *et al.* reported an electrochemical biosensor to detect the influenza H1N1 virus.[77] CdSeTes quantum dots (QDs) were used for signal generation, whereas a synthesized gold nanoparticle−magnetic nanoparticle−carbon nanotube (AuNP−MNP−CNT) composite was used to magnetically separate virus particles from the sample solution. To synthesize MNP,

ferric chloride tetrahydrate and ferric chloride were dissolved in a mixture of ammonia and gallic acid solution. Then, $HAuCl_4$ and the MWCNT mixture in water were added to the MNP solution. GA induced Au ions to form AuNPs on the MWCNT surface; thus AuNP–MNP–CNT was synthesized. Antibodies specific to the influenza H1N1 virus were immobilized to QDs and AuNP–MNP–CNT via EDC/NHS to obtain ab-QDs and ab-AuNP–MNP–CNT. After influenza H1N1 antigens were added to the ab-AuNP–MNP–CNT mixture, ab-QDs were immobilized to form ab-QDs–virus–ab-AuNP–MNP–CNT sandwich structures to separate the target analyte in the sample solution. Finally, immunocomplex and hydrochloric acid were sequentially drop-cast on SPCE to cause the cleavage of Cd^{2+} ions on QDs. DPV was used to detect the influenza H1N1 antigen and the LOD was 13.66 fg ml^{-1} within the linear range between 1 fg ml^{-1} and 1 μg ml^{-1}. The stability of the developed sensor was up to three weeks. Also, influenza H1N1 was detected in human serum albumin with a correlation coefficient of 0.99.

3. Nucleic-acid-based Electrochemical Biosensors

Respiratory viruses have genomes that include specific genetic information used as a biomarker by nucleic acid-based biosensors, whereas primers designed as complementary base pairs of target nucleic acid are used as biorecognition elements.[2] DNA or RNA probes are immobilized to the electrode surface via a series of modifications. In the presence of target nucleic acids in samples, the electrochemical response of electrodes changes due to the specific binding between the probe and the target nucleic acids.[24] Nucleic acid sequences are extracted and amplified to develop a nucleic-acid-based biosensor. The extraction of nucleic acid sequences is achieved by the lysis of respiratory viruses.[78] There are several methods for the desired target nucleic acid amplification, such as isothermal, thermal cycling, and rolling circle amplification.[79] Whereas the temperature has to be controlled in thermal cycling amplification, this process is not necessary in isothermal amplification.[2]

Silva *et al.* developed 3D-printed electrodes modified with AuNPs to detect SARS-CoV-2 [Fig. 2(A)].[80] The electrodes were fabricated using graphene polylactic (G-PLA) filaments and a 3D printer. The AuNPs were used to modify the electrode surface via electrodeposition. Then, the complementary DNA (cDNA) capture sequence was incubated on the modified electrode via thiol groups with the use of 2-mercaptoethanol in TRIS buffer. After the hybridization occurred between the target sequence and the cDNA capture sequence, SARS-CoV-2 cDNA was detected by SWV. The LOD was found to be 0.30 μmol L^{-1}. The biosensor was applied to artificial urine and human serum with a sensitivity of 9.318 μA $mmol^{-1}$ and recovery values of 98.0–103.0% and 95.0–105.0%, respectively. This biosensor is advantageous because it enables low-cost, automated, and simple fabrication of the electrodes.

Pina-Coronado *et al.* developed an electrochemical biosensor for detecting SARS-CoV-2-related DNA sequences.[81] Methylene-blue-modified carbon nanodots (MB-CDs) were synthesized using an L-arginine, methylene blue chloride, and 3,3′-diamino-N-methyldipropylamine mixture in a microwave and then purified by dialysis for seven days. The gold nanostructures (AuNs), a mixture of AuNPs, and gold nanotriangles (AuNTs) were synthesized using the seed-mediated growth procedure in 45 min.[82] Synthesized AuNs were

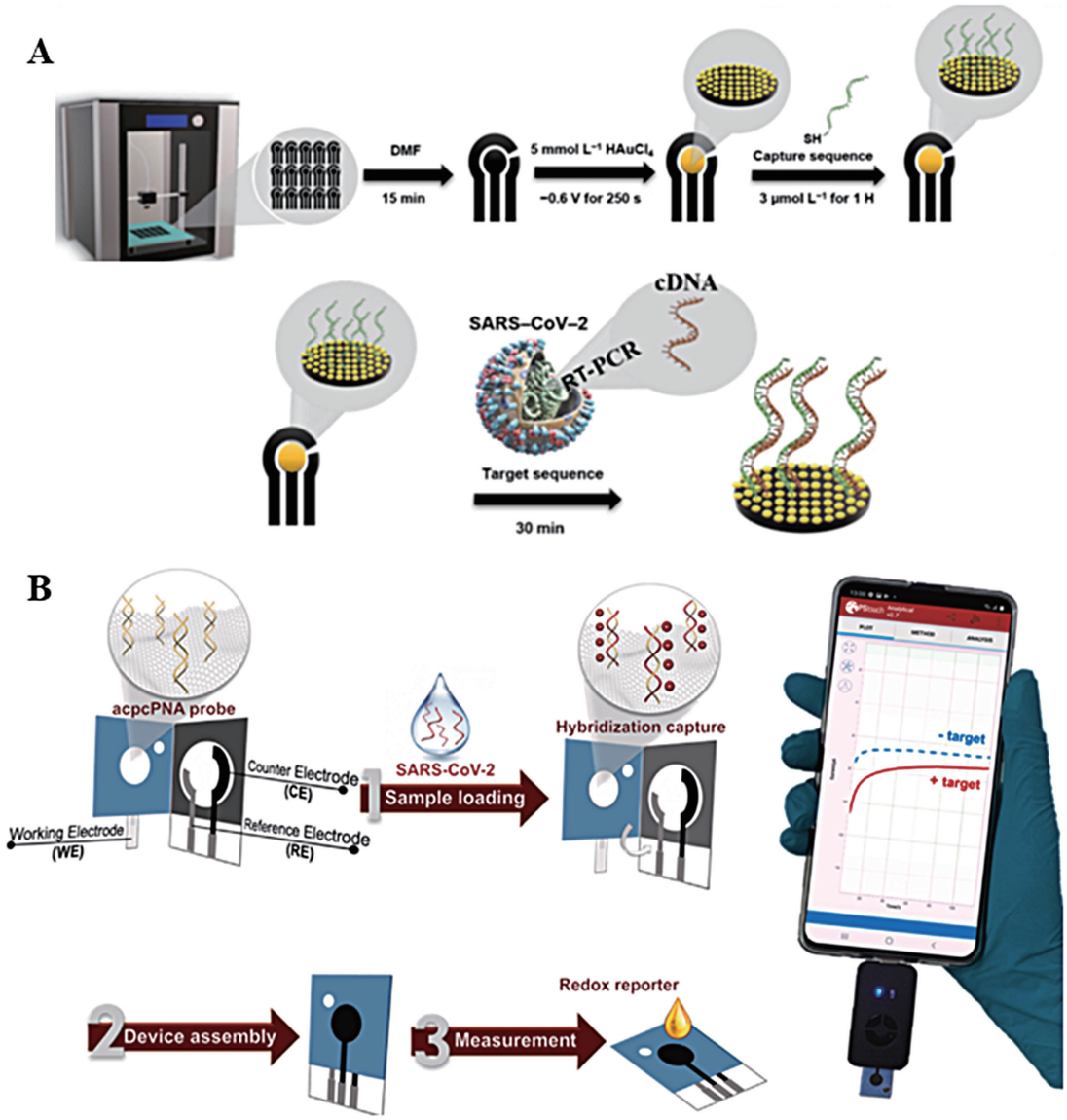

Fig. 2. (Color online) (A) (i) Schematic representation of the sensor for the detection of SARS-CoV-2, (ii) schematic representation of the hybridization stages of the sensor. Adapted with permission from Ref. 80 (Copyright 2022, Elsevier B.V.). (B) Detection mechanism of PNA-based ePAD sensor connected with a smartphone-based potentiostat. Adapted with permission from Ref. 84 (Copyright 2023, Elsevier B.V.).

modified by spraying on the Au SPE surface using an airbrush. Then, a thiol-modified probe was added on the AuNs via drop-casting. The probe-SH/AuNs/AuSPE captured the target sequence obtained from the ORF1ab of SARS-CoV-2, and SARS-CoV-2 was detected using DPV with an LOD of 2.2 aM. While AuNs increased the sensitivity of the biosensor, MB-CDs were used as selective redox indicators. In addition, it was possible to recognize single nucleotide polymorphisms. The recovery was found to be 103.6% for human serum. In another study, Kaci *et al.* developed a AuNT-based biosensor for the detection of a specific DNA sequence of the RNA-dependent RNA polymerase (RdRp) gene of SARS-CoV-2.[83] The AuNTs synthesized by

a seed-mediated growth method and AuNts were used to modify the working electrode surface.[82] The synthesized AuNTs were sprayed on the SPCE, and the thiolated DNA probe was immobilized via drop-casting. After the hybridization step, DPV was applied and the LOD was found to be 22.2 fM. The sensing could be carried out without the amplification step at the POC owing to its portable and Wi-Fi-supported commercial read-out device.

In a recent study, Lomae *et al.* developed an ePAD biosensor for detecting SARS-CoV-2 DNA [Fig. 2(B)].[84] The electrodes were fabricated via screen-printing. While carbon graphene ink was used for the fabrication of the working and counter electrodes, silver/silver chloride (Ag/AgCl) ink was used for the reference electrode. As a biological recognition component to capture the target cDNA, pyrrolidinyl peptide nucleic acid (acpcPNA) was synthesized by solid-phase peptide synthesis and modified to the working electrode surface owing to the covalent bonding between aldehyde groups and amino groups.[85] In the presence of the target cDNA, hybridization of the acpcPNA probe blocks the redox reporter. The LOD was found to be 1.0 pM within the linear range between 0.1 and 200 nM using CA. The applicability of the ePAD was tested in artificial saliva samples and the recovery values were 96.5–104.5%. In addition, it was tested with swab samples taken from 10 different volunteers, seven of whom were COVID-19 patients, and it was found that the biosensor showed 100% specificity and sensitivity. The developed sensor has a high sensitivity to the N gene of SARS-CoV-2 owing to the highly selective binding between PNA and DNA.

The clustered regularly interspaced short palindromic repeats (CRISPR) technology, which was developed on the basis of the immune system of prokaryotic bacteria, was developed in 2020.[86] This technology has attracted attention in biosensing applications owing to its high sensitivity and specificity and its programmability in nucleic acid detection. Zhang *et al.* reported a pH-induced regenerative electrochemiluminescence (ECL) biosensor to detect the RdRp gene of SARS-CoV-2 from clinical swab samples.[87] At first, Au-g-C_3N_4 nanoparticles were synthesized by allowing reactions among $HAuCl_4$, g-C_3N_4, and $NaBH_4$ in an ice bath for 20 min, followed by the addition of sodium citrate. After that, DNA tetrahedron structures were prepared using four single-stranded DNAs (T1, T2, T3, and T4) in Tris(2-carboxyethyl) phosphine hydrochloride (TCEP) solution. Au-g-C_3N_4 NPs were drop-cast on the GCE surface and then Au-g-C_3N_4/GCE was incubated in DNA tetrahedron solution. Thus, Au-g-C_3N_4/GCE was modified with DNA tetrahedrons. The ECL response of the biosensor occured because of the signal amplification reaction with the SARS-CoV-2 RNA-gene-converted cDNA sequence. Owing to the DNA cleavage, the EIS signal was generated for the detection of SARS-CoV-2. Swab samples were used to detect SARS-CoV-2 via EIS by applying the scan rate of 0–1.5 V with the relative standard deviation (RSD) of 1.7%, and the LOD was 43.70 aM. The biosensor showed good recoveries between 99.26 and 101.9%.

Wu *et al.* reported a CRISPR/Cas12a-based electrochemical biosensor for the detection of SARS-CoV-2.[88] The E gene of the SARS-CoV-2 sequence was chosen as the target sequence, and RNA reverse transcription recombinase polymerase amplification (RT-RPA) was used to obtain target DNA fragments. Moreover, the CRISPR/Cas12a system was based on single-stranded DNA (ssDNA) trans-cleavage formation in the presence of cas12, target DNA, and crRNAs. SPCE was used as the working electrode and modified with a mixture of synthesized

ceric oxide (CeO_2) nanorods and polyethyleneimine in ethanol and commercial fc-labeled ssDNA via drop-casting. Then, the CRISPR/CAS 12a solution consisting of a mixture of CRISPR/CAS 12a, crRNAs (1,2,3,6), RNase inhibitors, and E gene DNA fragments was drop-cast on the electrode surface. ssDNA was allowed to be trans-cleaved on the electrode surface for 60 min. The linear range of E gene detection was determined as 2×10^{-8}–5×10^{-5} ng μL^{-1} with an LOD of 0.27 copies μL^{-1} in clinical samples using DPV. The selectivity of the biosensor to SARS-CoV-2 was tested in the presence SARS-CoV-1, MERS-CoV-1, and human coronavirus (HCoV)-HKU1 pseudovirus samples, and no crosstalk was found. RT-qPCR was used to validate the biosensor, and the detection results agreed with the RT-qPCR results.

Yang *et al.* reported a graphene/CRISPR-endonuclease-deficient cas9 (dCas9)-based electrochemical biosensor for the detection of delta variants of SARS-CoV-2 in clinical samples.[89] At first, graphene was dispersed in a chitosan medium and drop-cast on a Au electrode surface. Then, dCas9 was immobilized on the modified electrode surface with EDC/NHS coupling, followed by incubation with sgRNA solution. The electrode was incubated with synthesized $[Ru(phen)_2dppz]BF_4$, and DPV was applied to SARS-CoV-2 detection. $Ru(phen)_2Cl_2$ and dipyrido[3,2-a:2′,3′-c]phenazine were synthesized to obtain $[Ru(Phen)_2dppz]BF_4$. To synthesize $Ru(phen)_2Cl_2$, $Ru(phen)_2Cl_2RuCl_3{\cdot}nH_2O$1.10-phenanthroline and lithium chloride were dissolved in N, N-dimethylformamide (DMF). The LOD was found to be 1.2 pM within the linear range between 4 pM and 4 nM using DPV. The detection capability of the developed biosensor was confirmed in clinical samples by PCR with recovery values between 93.8 and 98.7%. The developed biosensor can sensitively detect the SARS-CoV-2 delta variant.

Wu *et al.* reported an electrochemical CRISPR-based biosensor for the detection of SARS-CoV-2 delta variants (Fig. 3).[90] A Au electrode was modified with AuNPs via electrochemical deposition by applying CA at 0.5 V in $HAuCl_4$ solution for 300 s. Commercial methylene blue-single-stranded DNA (MB-ssDNA) was immobilized on the electrode surface with the use of EDTA. Cas12a-crRNA duplex was added to the target DNA to form a Cas12a-crRNA-target DNA triplex, and then the Cas12a-crRNA-target DNA triplex was drop-cast on an MB-ssDNA-modified Au electrode. SWV was used to detect the SARS-CoV-2 delta variant, which is based on a Cas12a-mediated cleavage. The linear range of detection was determined as 100 fM–10 nM, whereas the LOD was 50 fM. The biosensor showed high specificity to the delta variant and remained stable for one week. In another study, Ji *et al.* reported an electrochemical biosensor that detects SARS-CoV-2 RNAs in nasopharyngeal samples.[91] In this study, a self-actuating molecular electrochemical system (MECS) was generated inspired by Hydra and its tentacles. Graphene microelectrodes were fabricated via the thermally assisted bilayer lift-off process.[92] MECS was generated using nanostructure SARS-CoV-2 DNAs and modified with methylene blue. The graphene electrode was incubated in 1-pyrenebutanoic acid succinimidyl and MECS in polydimethylsiloxane. Then, MECS was anchored to the surface of the graphene electrode owing to the interaction between 1-pyrenebutanoic acid succinimidyl ester (PASE) and PDMS. SWV and DPV were used to detect SARS-CoV-2, and the LODs were 0.025 and 0.035 copies μL^{-1}, respectively. The linear range was 0.05–5 copies μL^{-1}. The biosensor was applied to clinical samples with recoveries of ~100%.

In another study, Zhao *et al.* reported RNA-based electrochemical biosensors to detect SARS-CoV-2.[93] A capture probe (CP), labeled signal probe (LP), and auxiliary probe (AP)

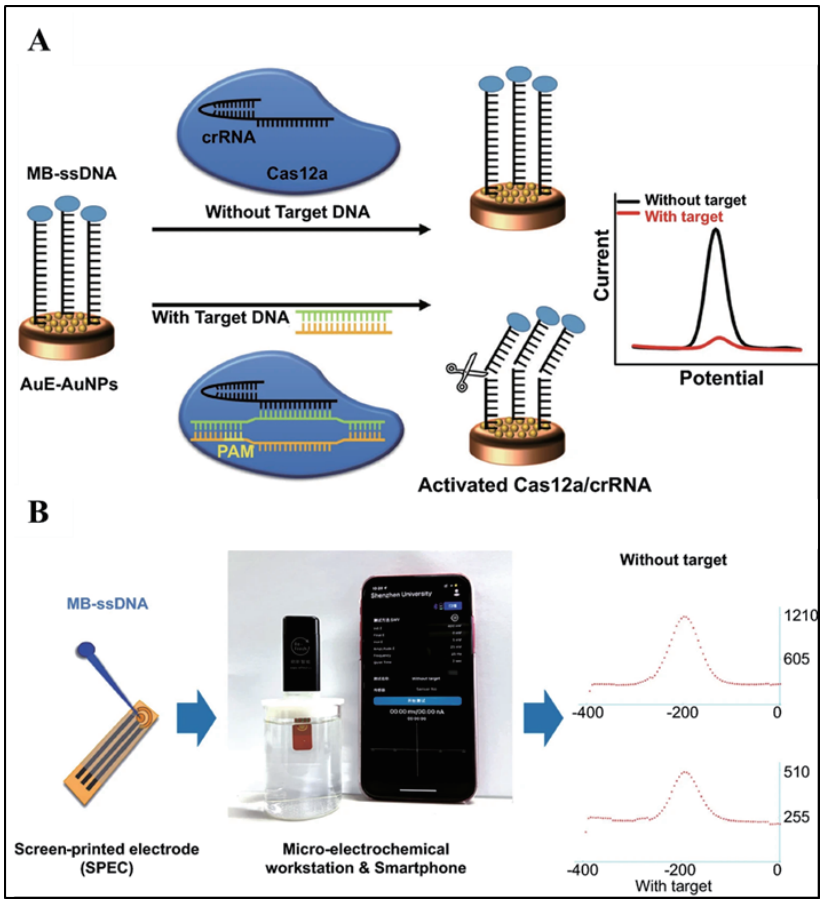

Fig. 3. (Color online) Schematic illustration of (A) AuNP-assisted E-CRISPR biosensor and (B) E-CRISPR application in POCT for SARS-CoV-2 Delta variant detection. Adapted with permission from Ref. 90 (Copyright 2022, Elsevier B.V.).

amplified from the ORF1ab gene by real-time PCR were used by adding LP to the target RNA sequence captured by CP to form the sandwich-type RNA recognition. To generate premix A, Au@Fe_3O_4 nanocomposites were synthesized. Then, the nanocomposite was incubated with CP, and the nonspecific binding was avoided by using hexane-1-thiol. To generate premix B, Au@p-sulfocalix 8 arene (SCX8)–reduced graphene oxide (RGO)–toluidine blue (TB) nanocomposites were synthesized and modified using a mixture of LP p-sulfocalix[8]arene and GO in water. Then, $HAuCl_4$ and TB were added to the solution to obtain Au@SCX8–RGO–TB, which was drop-cast on the electrode surface. After SARS-CoV-2 RNAs were extracted from the clinical COVID-19 patients' sample, they were mixed with premix A and premix B. The final mixture was drop-cast on the surface of commercial SPCE, and DPV was used for SARS-CoV-2 detection. The linear range was determined as 10^{-17} to 10^{-12} M with an LOD of 200 copies ml^{-1} in various clinical samples (sputum, throat swab, urine, feces, plasma, serum, whole blood, oral swab, and saliva). Owing to the use of sandwich-type RNA recognition, there is no need for RNA amplification or reverse transcription.

Heo *et al.* developed an electrochemical device based on the trans-cleavage activity of CRISPR/Cas13a for the detection of SARS-CoV-2 virus.[31] A nanocomposite and gold

nanoflower (AuNF) were used to improve the sensitivity of the biosensor. The nanocomposite was synthesized by mixing graphene nanoplatelets, MoS_2NSs, and chitosan (CHT). The reporter RNA (reRNA) was tagged with biotin and methylene blue as a redox probe. The reRNA was immobilized on a commercial SCPE via streptavidin–biotin interaction. The RNase function of Cas13a was activated once the SARS-CoV-2 RNA was captured by the Cas13a-crRNA complex. The Cas13a-crRNA complex was enzymatically activated and then incorporated into the reRNA-conjugated electrochemical sensor. Finally, the Cas13a-crRNA complex cleaved reRNA. Once reRNA was trans-cleaved from the Cas13a-crRNA complex, DPV was applied. The ORF and S genes of the SARS-CoV-2 virus were detected in the linear range between 1.0×10^1 and 1.0×10^5 fg mL^{-1} with LODs of 4.4×10^{-2} and 8.1×10^{-2} fg mL^{-1}, respectively. Furthermore, SARS-CoV-2 RNA spiked in artificial saliva was used to test the biosensor, and the recovery values were 109.4–111.3% and 96.5–101.2% for the ORF and S genes, respectively. The biosensor has an advantage that it can detect the SARS-CoV-2 RNA complex sample matrix without the need of viral RNA purification.

Kashefi-Kheyrabadi *et al.* developed a nucleic acid amplification-free electrochemical biosensor for the detection of SARS-CoV-2.[94] The biosensor was based on the construction of four-way junction (4-WJ) hybridization specific to SARS-CoV-2 owing to the hybridization of the target RNA, mediator-labeled m-strand, and associated f-strand to the DNA hairpin (UDH) probe. S and Orf1ab RNA sequences were determined as target RNA for SARS-CoV-2 detection. Dual SPGEs were used as substrates for UDH probes. SPCE was electrochemically modified with Au to generate a 3D gold nanoneedle-structured layer. Then, the thiolated UDH probe was modified to form a 4-WJ structure and incubated on the SPE surface. Target RNAs were produced using synthesized DNA templates via T7 transcription. Finally, the UDH probe was hybridized with RNA targets, redox mediator-labeled m-strand, and associated f-strand. The performance of the biosensor was confirmed with various respiratory specimen samples, including 16 SARS-CoV-2-positive and five SARS-CoV-2-negative samples. Electrochemical measurements were carried out using SWV. The linear range of S and Orf1ab gene detection was 1×10^{-16} to 1×10^{-11} M for clinical nasopharyngeal samples. The LODs were 5.0 and 6.8 ag μL^{-1} for S and Orf1ab genes, respectively. The developed biosensor remained stable for up to two weeks.

Deng *et al.* developed an electrochemical sensing platform using a target-triggered cascade signal amplification strategy for SARS-CoV-2 RNA detection.[95] A Au electrode was polished with alumina powder and sonicated to prepare the electrode for use in detection. Then, the surface of the electrode was treated with tris(2-carboxyethyl)phosphine hydrochloride (TCEP). Then, the electrode was incubated for 2 h. During these processes, EDTA was used as a crosslinker and MCH was used as a blocking agent. The modified electrode was then hybridized with HP2 and its target for 2 h. Then, the electrode was incubated with a deoxyribonucleotide mixture (dNTP) and terminal deoxynucleotidyl transferase (TdT) for 1 h and made ready for detection. The LOD was 45 fM within the linear range of 0.1–3000 pM. The SARS-CoV-2 RNA spiked in diluted saliva was tested and compared with those spiked in Tris-HCl.

4. Aptamer-based Electrochemical Biosensors

Aptamers, which are short oligonucleotides, consist of single-stranded DNA or RNA.[96] Aptamers are used as biorecognition elements in biosensors and bind to target molecules with high specificity. In addition, they are advantageous over antibodies because they are inexpensive and have simple steps for synthesis.[97] They are also easily modified and have a shorter manufacturing time than antibodies. Since aptamers are chemically synthesized by the systematic evolution of ligands by the exponential enrichment (SELEX) method, various groups can be used in their modifications.[98] For example, Ramanathan *et al.* reported a carbon-nanodiamond-modified aptasensor for the detection of SARS-CoV-2 nucleocapsid protein.[99] A commercial Au interdigitated electrode (AuIDE) was modified by the amino-silanization of hydroxyl groups in potassium hydroxide solution. Then, 1,1′carbonyldiimidazole (CDI)-modified diamonds were synthesized using commercial diamond powder and CDI solution, followed by incubation on the electrode surface for 2 h. Then, the commercial amine-ended nucleocapsid protein (NCP) aptamer was immobilized on the working electrode and ethanolamine was used as a blocking agent. The linear range of detection was determined to be between 1 fM and 100 pM with an LOD of 0.389 fM by EIS in NCP-spiked human serum.

Han *et al.* developed the CRISPR/Cas12a-derived aptasensor to detect the SARS-CoV-2 N protein.[100] A methylene blue-labeled poly-adenine DNA sequence was immobilized on a Au electrode surface. After that, an arched probe was generated by hybridizing an activator strand with the N aptamer. The aptamer attached to its target and released the activator strand in the presence of SARS-CoV-2 N. Then, the activator released from the arched probe activated the trans-function activity of the CRISPR/Cas12a system. The trans-cleavage activity of Cas12a was detected by DPW. The linear response was in the concentration range of 50 pg ml^{-1}–100 ng ml^{-1} and LOD was 16.5 pg ml^{-1} . The applicability of the biosensor was tested to detect nucleocapsid proteins in tap water, milk, and serum samples with an average recovery value of 101.3 ± 2.0%.

Yang *et al.* reported a single-nanoparticle collision electrochemistry (SNCE)-based biosensor to detect H7N9 AIV (Fig. 4).[101] MNPs, aptamer (apt), ssDNA1, and its complementary sequence ssDNA2 were used to produce magneto-nanosensors (MNs)-ssDN2-AuNPs and MNs-apt-ssDNA1. MNs were activated by EDC/NHS, followed by the addition of streptavidin (SA). Then, biotin-modified aptamers were added to MNs-SA. As a result of the conjugation between SA and biotin, MNs-apt was formed. Then, ssDNA1 was added to the solution and conjugated with aptamers. To produce MNs-ssDN2-Au NPs, ssDNA2 was mixed with PBS and TRIS, followed by the addition of the MNs-SA solution. Then, the MNs-ssDN2 solution was incubated with AuNPs. The H7N9 AIV-containing sample was added to the MNs-apt-ssDNA 1 solution. The ssDNA1 was cleaved from MNs-apt-ssDNA1 because of the recognition of H7N9 AIV by the aptamers. Then, the ssDNA1 cleaved solution was reacted with the MNs-ssDN2-Au NP solution and ssDNA1 was conjugated to ssDNA2. After that, a magnet was used to remove the supernatant. Nt.AlwI, a nicking endonuclease, was added to the cleaved AuNPs from MNs-ssDN2-AuNPs in the presence of the conjugated ssDNA1-ssDNA2. The supernatant AuNPs were separated from the medium using a magnet and drop-cast on the Au electrode. CA was used for the detection of H7N19 AIV viruses. While the linear range of detection was determined

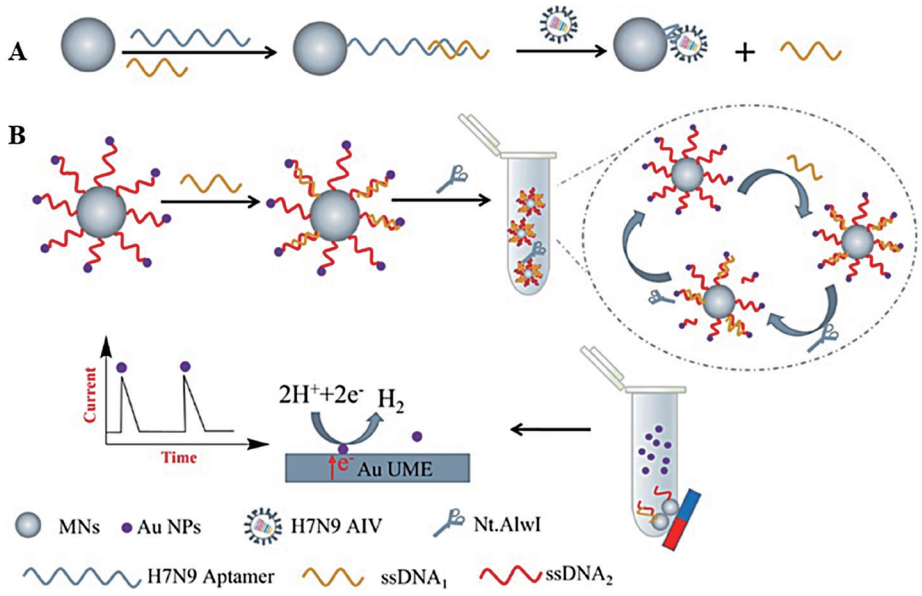

Fig. 4. (Color online) Schematic representation of (A) ssDNA1 release and (B) nicking endonuclease Nt.AlwI-mediated target recycling and AuNP release for the electrochemical single-nanoparticle collision measurement of H7N9 AIV. Adapted with permission from Ref. 101 (Copyright 2022, American Chemical Society).

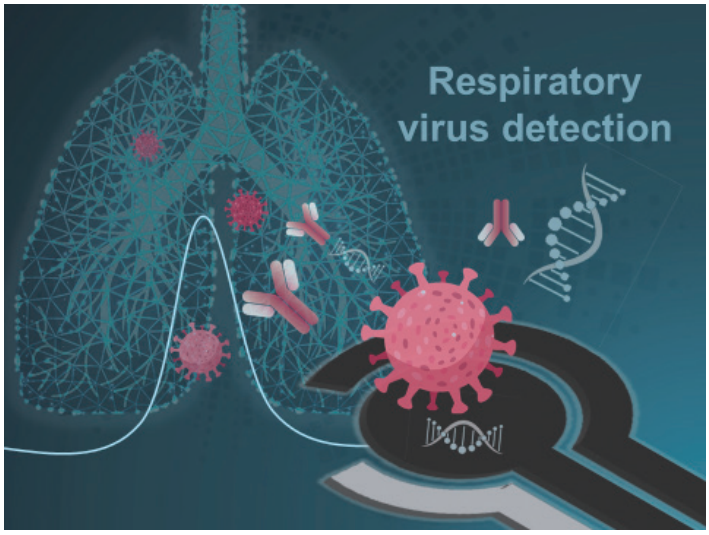

Fig. 5. (Color online) Graphical abstract.

as 0.2 pg ml^{-1}–200 ng ml^{-1}, the LOD was determined as 24.3 fg ml^{-1}. However, the biosensor should be validated using clinical samples.

Kim *et al.* developed an electrochemical and surface-enhanced Raman spectroscopy (EC/SERS)-based biosensor using a multifunctional DNA aptamer and graphene oxide molybdenum disulfide (GO-MoS_2).[102] The MERS aptamer, GO-MoS_2 nanocomposite, and MERS-nanovesicle (NV) were synthesized. At first, GO was introduced into MoS_2 via electrostatic

Table 1
Summary of characteristics of electrochemical biosensors for respiratory viruses.

Active Layer	Virus	Technique	LOD	Linear Range	Ref.
Au/SAM/rSpike electrodes	SARS-CoV-2	CV and EIS	2.53 nM (CV) 1.99 Nm (EIS)	N/A	46
Au electrode	SARS-CoV-2	EIS	1.1×10^5 gcn mL^{-1}	10^4–10^9 virus particles mL^{-1}	47
Au/CHS/Ab1	SARS-CoV-2	DPV	0.08 pg · mL^{-1}	$0.2–2.10 \times 10^5$	48
SPE	SARS-CoV-2	CA	1 fg mL^{-1}	0.01−10000 pg mL^{-1}	50
Graphene oxide	SARS-CoV-2	SWV	1 ng mL^{-1}	N/A	51
AJP graphene electrode	SARS-CoV-2	EIS	22.91 ± 4.72 pg mL^{-1} (RPD protein) 110.38 ± 9.00 pg mL^{-1} (spike S1)	1 to 1000 ng mL^{-1}	52
S-D electrodes	SARS-CoV-2	IDS	4.12 fg mL^{-1}	0.1 fg mL^{-1} to 5.0 pg mL^{-1}	53
SPCE	SARS-CoV-2	CA	68 equiv PFU mL^{-1}	5 to 10^6 PFU mL^{-1}	54
Stencil-printed carbon electrode	SARS-CoV-2	CA	lower than 5 ng mL^{-1}	0 to 100 ng mL^{-1}	55
SPCE	H5N1 H7N9 H9N2	DPV	55.7 (pg mL^{-1}) for H5N1 HA (0.95 pM) 99.6 (pg mL^{-1}) for H7N9 HA (1.69 pM) 54.0 (pg mL^{-1}) for H9N2 HA (0.72 pM)	100 pg mL^{-1} to 100 ng mL^{-1}	56
CNF/SPCE	MERS-CoV	SWV	0.07 pg mL^{-1}	0.1 pg mL^{-1} to 1 μg mL^{-1}	57
Magnetic bead/ carbon black/screen-printed electrode	SARS-CoV-2	DPV	19 ng mL^{-1} (S-Protein) 8 ng mL^{-1} (N-Protein)	N/A	58
Au-Pd/GCE	SARS-CoV-2	DPV	0.01 ng mL^{-1} to 1000 ng mL^{-1}	0.0072 ng mL^{-1}	59
SCPE	SARS-CoV-2	DPV	0.53 ng mL^{-1} (S1) 0.75 ng mL^{-1} (S2)	1.0–200 ng mL^{-1} (S1) 2.5–100 ng mL^{-1} (S2)	60
CNC/SPGE	SARS-CoV-2	DPV	2.0 fg mL^{-1}	0.1 pg mL^{-1} to 500 ng mL^{-1}	63
Ab/CNC/SPGE	SARS-CoV-2	DPV	2.0 fg mL^{-1}	0.1 pg mL^{-1} to 500 ng mL^{-1}	63
Au/TFME	SARS-CoV-2	SWV	64 fM (Real samples) 15 fM (PBS)	0–400 fM (Real samples)	64
SPCE	SARS-CoV-2	CV and EIS	1.065 fg mL^{-1}	N/A	65
Pt/Ti electrode bare DIDC chip	SARS-CoV-2	DC	1 fg mL^{-1}	1.0 mg mL^{-1} to 1.0 fg mL^{-1}	66
AuE	SARS-CoV-2	SWV	7.44 pM (PBS) 2.96 pM (Artificial saliva)	0.4 ng mL^{-1} to 400 ng mL^{-1}	67
SPCE	SARS-CoV-2 A(H1N1)	Amperometry	1.12 unit mL^{-1} for A(H1N1) 0.15 ng mL^{-1} for SARS-CoV-2	4−64 unit mL^{-1} for A(H1N1) 0.15−100 ng mL^{-1} for SARS-CoV-2	68
GPT/PLA electrode	SARS-CoV-2	CV	1.36 nmol L^{-1}	5.0 to 75.0 nmol L^{-1}	70
GNP/SPEs	SARS-CoV-2	DPV	12 ng mL^{-1}	0.5–5 μg mL^{-1} range	72
Boron-doped diamond	SARS-CoV-2	EIS	1 fg mL^{-1}	N/A	73

Table 1 (continued)
Summary of characteristics of electrochemical biosensors for respiratory viruses.

Active Layer	Virus	Technique	LOD	Linear Range	
GOx/Ti_3C_2/pAb	H1N1	pH-meter-based electrochemical measurements	1.3 ng mL^{-1}	0.01 μg mL^{-1} to 100 μg mL^{-1}	75
Ab-QDs-virus-Ab-AuNP-MNP-CNT / Screen-printed carbon electrode	HH1N1	DPV	13.66 fg mL^{-1}	1 fg mL^{-1} to 1 μg mL^{-1}	77
Au-modified G-PLA	SARS-CoV-2	SWV	0.30 μmol L^{-1}	N/A	80
AuSPE	SARS-CoV-2	DPV	2.2 aM	N/A	81
AuNT/CSPE.	SARS-CoV-2	DPV	22.1 fM	N/A	83
Pyrrolidinyl peptide nucleic-acid-modified paper-based electrode	SARS-CoV-2	EIS and CV	1.0 pM	0.1 to 200 nM	84
Au-g-C3N4CE	SARS-CoV-2	Electrochemical luminescence	43.70 aM	N/A	87
CRISPR/CAS 12-SPCE	SARS-CoV-2	DPV	5.0×10^{-9} ng μL^{-1} 0.27 copies μL^{-1} (Clinical samples)	2.0×10^{-8} to 5.0×10^{-5} ng μl L^{-1}	88
Gold electrode modified with graphene and CRISPR-dCas9	SARS-CoV-2 (Delta variant)	DPV	1.2 pM	4 pM to 4 nM	89
MB-ssDNA-modified AuE-AuNPs	SARS-CoV-2 (Delta variant)	SWV	50 fM	100 fM to 10 nM	90
MECS-modified graphene microelectrode	SARS-CoV-2	SWV and DPV	0.025 copies μL^{-1} SWV, 0.035 copies μL^{-1} DPV	0.05 to 5 copies μL^{-1}	91
SPCE	SARS-CoV-2	DPV	200 copies mL^{-1}	10^{-17} to 10^{-12} M	93
AuNF/NC/SPCE	SARS-CoV-2	CV	4.4×10^{-2} fg mL^{-1} for ORF gene 8.1×10^{-2} fg mL^{-1} for S gene	1.0×10^{-1} to 1.0×10^{5} fg mL^{-1}	31
GN/SPGE	SARS-CoV-2	SWV	5.0 ag μL^{-1} (S) 6.8 ag μL^{-1} (Orf1ab)	1×10^{-16} to 1×10^{-11} M	94
Hairpin-modified gold electrode	SARS-CoV-2	DPV and EIS	45 fM	0.1 to 3000 pM	95
AuIDE	SARS-CoV-2	EIS	0.389 fM 1 fM to 100 pM	99	
Poly-A-MB-modified gold electrode	SARS-CoV-2	DPV and EIS	16.5 pg mL^{-1}	0.05–100 ng mL^{-1}	100
Au UME	H7N9 AIV	CA	24.3 fg mL^{-1}	0.2 pg mL^{-1} to 200 ng mL^{-1}	101
GO-MoS2 nanocomposite-modified Au electrode	MERS-CoV	EC/SERS	0.405 pg mL^{-1} for PBS 0.645 pg mL^{-1} for diluted 10% saliva	N/A	102

interaction to produce the nanocomposite. The MERS aptamer was synthesized by the SELEX method. In this method, commercial EZ-Link Sulfo-NHS-LC-Biotin reacted with MERS S1 (spike 1) protein. Then, the MERS S1 protein was immobilized by adding commercial streptavidin magnetic beads. The synthesized MERS aptamer and commercial multifunctional (MF) DNA fragments were combined to form a multifunctional aptamer. The aptamer was linked to the DNA three-way junction structure and immobilized on a GO-MoS_2 nanocomposite

via peptide bonds. Then, cysteamine was drop-cast on the electrode surface to form a thin-film layer, whereas EDC/sulfo-NHS was used as a crosslinker. After that, the MF MERS aptamer was dropcast on the GO-MoS_2-modified electrode. The LODs were found to be 0.405 and 0.645 pg ml^{-1} for the spiked PBS solution and 10% saliva sample, respectively, by the EC/SERS technique.

5. Conclusions

Conventional detection methods are insufficient for the detection of respiratory viruses; therefore, studies have recently been focused on electrochemical biosensors owing to their superior characteristics, including high selectivity and sensitivity, the need for low sample volume, simplicity, fast response, and POC capability. In this review, the fabrication and modification steps of antibody-based, nucleic-acid-based, and aptamer-based biosensors were overviewed and discussed in detail.

Nucleic-acid-based biosensors have advantages such as high selectivity and sensitivity owing to the specific binding between the probes and the target analyte. However, the extraction of nucleic acids and the identification of target-specific regions can be costly and challenging since the specificity of the probe depends on the sequence and hybridization conditions such as buffer composition and temperature. In addition, nucleic acids have stability issues for long-term use. Antibodies are complex and unstable, and their synthesis is expensive compared with nucleic acids. In addition, the use of antibodies for the detection of small targets, including metal ions and drugs, can be misleading, and antibodies also tend to produce crosstalk. While mAb is more specific than pAb, pAb is less expensive than mAb. Antibody-based biosensors offer reversible binding, stepwise reaction, and high specificity to surface chemical groups. Therefore, antibody-based biosensors are one of the most adaptable and easily accessible biosensors for detecting respiratory viruses. The use of aptamers consisting of single-stranded oligonucleotide chains is highly preferred owing to their high affinity and specificity. Besides, they can be synthesized in a short time at a low-cost. Since aptamers can be denatured at high temperature, they can be generated with high quality via chemical synthesis and used for the modification of biosensors.

While nanomaterials were used in the modification of biosensors to increase stability and sensitivity, microarray systems reduce the cost of biosensors owing to their ability to simultaneously detect respiratory viruses. Although various electrochemical biosensors offer sensitive detection of respiratory viruses, some of the aforementioned biosensors need to be tested using real samples to prove their applicability.

Acknowledgments

This work is supported by the Scientific and Technological Research Council of Turkey (TUBITAK) (Grant nos. 122Z721 and 120N615). Additional support was provided by the National Institutes of Health, USA (Grant no. R01EB031510).

References

1 M. Moriyama, W. J. Hugentobler, and A. Iwasaki: Annu. Rev. Virol. **7** (2020) 83. https://doi.org/10.1146/annurev-virology-012420-022445
2 T. Ozer and C. S. Henry: Trends Anal. Chem. **144** (2021) 116424. https://doi.org/10.1016/j.trac.2021.116424
3 N. Zhang, L. Wang, X. Deng, R. Liang, M. Su, C. He, L. Hu, Y. Su, J. Ren, F. Yu, L. Du, and S. Jiang: J. Med. Virol. **92** (2020) 408. https://doi.org/10.1002/jmv.25674
4 A. Parihar, P. Ranjan, S. K. Sanghi, A. K. Srivastava, and R. Khan: ACS Appl. Bio Mater. **3** (2020) 7326. https://doi.org/10.1021/acsabm.0c01083
5 M. Khoury, J. Cuenca, F. F. Cruz, F. E. Figueroa, P. R. M. Rocco, and D. J. Weiss: Eur. Respir. J. **55** (2020) 2000858. https://doi.org/10.1183/13993003.00858-2020
6 T. Ozer, B. J. Geiss, and C. S. Henry: J. Electrochem. Soc. **167** (2019) 037523. https://doi.org/10.1149/2.0232003JES
7 T. Ozer and C. S. Henry: Trends Anal. Chem. **144** (2021) 116424. https://doi.org/10.1016/j.trac.2021.116424
8 Y. Rasmi, X. Li, J. Khan, T. Ozer, and J. R. Choi: Anal. Bioanal. Chem. **413** (2021) 4137. https://doi.org/10.1007/s00216-021-03377-6
9 M. Azar, M. Zavvari, P. Mohammadi, and Y. Zehforoosh: J. Nanophotonics **12** (2018) 046002. https://doi.org/10.1117/1.JNP.12.046002
10 H.-Y. Li, W.-J. Jia, X.-Y. Li, L. Zhang, and C. Liu: J. Exp. Med. **9** (2020) 1671. https://doi.org/10.1080/22221751.2020.1792352
11 Y. Rasmi, X. Li, J. Khan, T. Ozer, and J. R. Choi: Anal. Bioanal. Chem. **413** (2021), 4137. https://doi.org/10.1007/s00216-021-03377-6
12 M. M. Zareh, I. F. Ismail, and M. H. Abd El-Aziz: Electroanalysis **22** (2010) 1369. https://doi.org/10.1002/elan.200900550
13 J. M. Heraud, N. H. Razanajatovo, and C. Viboud: Lancet Glob. Health **7** (2019) e982. https://doi.org/10.1016/S2214-109X(19)30277-3
14 A. Lwoff and P. Tournier: Annu. Rev. Microbiol. **20** (1966) 45. https://doi.org/10.1146/annurev.mi.20.100166.000401
15 P. P. Nelson and N. G. Papadopoulos: Encyclopedia of Respiratory Medicine, C. Skevaki, Ed. (AP, London, 2020) 2nd ed., Chap. 4.
16 A. Siddharta, S. Pfaender, N. J. Vielle, R. Dijkman, M. Friesland, B. Becker, J. Yang, M. Engelmann, D. Todt, M. P. Windisch, F. H Brill, J. Steinmann, S. Becker, M. P. Alves, T. Piethschman, M. Eickmann, V. Thiel, and E. Steinmann: J. Infect. Dis. **215** (2017) 902. https://doi.org/10.1093/infdis/jix046
17 D. A. Tyrrell and S. H. Myint: Medical Microbiology, S. Baron, Ed. (UTMB, Galveston, 1996) 4th ed., Chap. 60.
18 K. V. Holmes: Encyclopedia of Virology, A. Granoff, and R. G. Webster, Eds. (AP, Cambridge, 1999) 2nd ed., pp. 291–298.
19 W. Tai, L. He, X. Zhang, J. Pu, D. Voronin, S. Jiang, Y. Zhou, and L. Du: Cell. Mol. Immunol. **17** (2020), 613. https://doi.org/10.1038/s41423-020-0400-4
20 P. Pokhrel, C. Hu, and H. Mao: ACS Sens. **5** (2020), 2283. https://doi.org/10.1021/acssensors.0c01153
21 V. M. Corman, O. Landt, M. Kaiser, R. Molenkamp, A. Meijer, D. K. Chu, T. Bleicker, S. Brünink, J. Schneider, M. L. Schmidt, J. E. Schmidt, D. G. Mulders, B. L. Haagmans, B. van der Veer, S. van den Brink, L. Wijsman, G. Goderski, J. L. Romette, J. Ellis, M. Zambon, M. Peiris, H. Goossens, C. Reusken, M. P. Koopmans, and C. Drosten: Eurosurveillance **25** (2020) 20000445. https://doi.org/10.2807/1560-7917.ES.2020.25.3.2000045
22 B. Alhalaili, I. N. Popescu, O. Kamoun, F. Alzubi, S. Alawadhia, and R. Vidu: Sensors **20** (2020) 6591. https://doi.org/10.3390/s20226591
23 T. Noda and Y. Kawaoka: Rev. Med. Virol. **20** (2010) 380. https://doi.org/10.1002/rmv.666
24 Z. Zhao, C. Huang, Z. Huang, F. Lin, Q. He, D. Tao, N. Jaffrezic-Renault, and Z. Guo: Trends Anal. Chem.**139** (2021) 116253. https://doi.org/10.1016/j.trac.2021.116253
25 Y. Yan, L. Chang, and L. Wang: Rev. Med. Virol **30** (2020) e2106. https://doi.org/10.1002/rmv.2106
26 A. Zumla, D. S. Hui, and S. Perlman: Lancet **386** (2015) 995. https://doi.org/10.1016/S0140-6736(15)60454-8
27 X. Lu, B. Whitaker, S. K. K. Sakthivel, S. Kamili, L. E. Rose, L. Lowe, E. Mohareb, E. M. Elassal, T. Al-sanouri, and A. Haddadin: J. Clin. Microbiol. **52** (2014) 67. https://doi.org/10.1128/JCM.02533-13
28 K. K. W. To, O. T. Y. Tsang, C. C. Y. Yip, K. H. Chan, T. C. Wu, J. M. C. Chan, W. S. Leung, T. S. H. Chik, C. Y. C. Choi, and D. H. D. Kandamby: Clin. Infect. Dis. **71** (2020) 841. https://doi.org/10.1093/cid/ciaa149
29 M. S. Ho, W. J. Chen, H. Y. Chen, S. F. Lin, M. C. Wang, J. Di, Y. T. Lu, C. L. Liu, S. C. Chang, and C. L. Chao: Emerg. Infect. Dis. **11** (2005) 1730. https://doi.org/10.3201/eid1111.040659

30 M. Sato, R. Saito, T. Sakai, Y. Sano, M. Nishikawa, A. Sasaki, Y. Shobugawa, F. Gejyo, and H. Suzuki: J. Clin. Microbiol.**43** (2005) 36. https://doi.org/10.1128/jcm.43.1.36-40.2005
31 W. Heo, K. Lee, S. Park, K. A. Hyun, and H. Jung: Biosens. Bioelectron. **201** (2022) 113960. https://doi.org/10.1016/j.bios.2021.113960
32 N. Kumar, N. P. Shetti, S. Jagannath, and T. M. Aminabhavi: J. Chem. Eng. **430** (2022) 132966. https://doi.org/10.1016/j.cej.2021.132966
33 Y. Tepeli and U. Anık: Sens. Actuators, B **254** (2018) 377. https://doi.org/10.1016/j.snb.2017.07.126
34 M. A. Abdul Ghani, A. N. Nordin, M. Zulhairee, A. Che Mohamad Nor, M. Shihabuddin Ahmad Noorden, M. K. F. Muhamad Atan, R. Ab Rahim, and Z. Mohd Zain: Biosensors **12** (2022) 666. https://doi.org/10.3390/bios12080666
35 D. Campos-Ferreira, V. Visani, C. Córdula, G. Nascimento, L. Montenegro, H. Schindler, and I. M. F. Cavalcanti: Biochem. Eng. J. **176** (2021) 108200. https://doi.org/10.1016/j.bej.2021.108200
36 H. O. Kaya, A. E. Cetin, M. Azimzadeh, and S. N. Topkaya: J. Electroanal. Chem. **882** (2021) 114989. https://doi.org/10.1016/j.jelechem.2021.114989
37 F. Ricci, G. Adornetto, and G. Palleschi, Electrochim. Acta **84** (2012) 74. https://doi.org/10.1016/j.electacta.2012.06.033
38 X. Luo, A. Morrin, A. J. Killard, M. R. Smyth: Electroanalysis **18** (2006) 319. https://doi.org/10.1002/elan.200503415
39 S. A. Lim and M. U. Ahmed: Immunosensors, M. U. Ahmed, M. Zourob, and E. Tamiya, Eds. (RSC Adv., Croydon, 2019).
40 E. Boel, S. Verlaan, M. J. Poppelier, N. A. Westerdaal, J. A. Van Strijp, and T. Logtenberg: J. Immunol. Methods **239** (2000) 153. https://doi.org/10.1016/S0022-1759(00)00170-8
41 N. S. Lipman, L. R. Jackson, L. J. Trudel, and F. Weis-Garcia: ILAR J. **46** (2005) 258. https://doi.org/10.1093/ilar.46.3.258
42 I. Tzouvadaki, J. Zapatero-Rodríguez, S. Naus, G. de Micheli, R. O'Kennedy, S. Carrara: Sens. Actuators, B Chem. **286** (2019) 346. https://doi.org/10.1016/j.snb.2019.02.001
43 S. A. Abid, A. A. Muneer, I. M. Al-Kadmy, A. A. Sattar, A. M. Beshbishy, G. E.-S. Batiha, and H. F. Hetta: Life Sci. **273** (2021) 119117. https://doi.org/10.1016/j.lfs.2021.119117
44 K. Tsumoto, K. Shinoki, H. Kondo, M. Uchikawa, T. Juji, and I. Kumagai: J. Immunol. Methods **219** (1998) 119. https://doi.org/10.1016/S0022-1759(98)00127-6
45 F. Zhang, Y. Chen, Y. Ke, L. Zhang, B. Zhang, L. Yang, and J. Zhu: Viruses **11** (2019) 58. https://doi.org/10.3390/v11010058
46 M. Drobysh, V. Liustrovaite, A. Baradoke, A. Rucinskiene, A. Ramanaviciene, V. Ratautaite, R. Viter, C.-F. Chen, I. Plikusiene, and U. Samukaite-Bubniene: Int. J. Mol. Sci. **23** (2022) 6768. https://doi.org/10.3390/ijms23126768
47 I. Ashur, J. Alter, M. Werbner, A. Ogungbile, M. Dessau, M. Gal-Tanamy, and S. Vernick: Talanta **239** (2022) 123147. https://doi.org/10.1016/j.talanta.2021.123147
48 A. Kowalczyk, A. Kasprzak, M. Ruzycka-Ayoush, E. Podsiadły, U. Demkow, I. P. Grudzinski, and A. M.Nowicka: Sens. Actuators, B **371** (2022) 132539. https://doi.org/10.1016/j.snb.2022.132539
49 A. Kasprzak, K. Fateyeva, A. Kowalczyk, and A. M. Nowicka: Anal. Chim. Acta **1108** (2020) 10. https://doi.org/10.1016/j.aca.2020.02.045
50 H. Zargartalebi, H. Yousefi, C. D. Flynn, S. Gomis, J. Das, T. L. Young, E. Chien, S. Mubareka, A. McGeer, and H.Wang: J. Am. Chem. Soc. **144** (2022), 18338. https://doi.org/10.1021/jacs.2c06192
51 A. Yakoh, U. Pimpitak, S. Rengpipat, N. Hirankarn, O. Chailapakul, and S. Chaiyo: Biosens. Bioelectron. **176** (2021) 112912. https://doi.org/10.1016/j.bios.2020.112912
52 C. C. Pola, S. V. Rangnekar, R. Sheets, B. M. Szydłowska, J. R. Downing, K. W. Parate, S. G. Wallace, D. Tsai, M. C. Hersam, C. L. Gomes, and J. C. Claussen: 2D Mater. **9** (2022) 035016. https://doi.org/10.1088/2053-1583/ac7339
53 M. A. Zamzami, G. Rabbani, A. Ahmad, A. A. Basalah, W. H. Al-Sabban, S. N. Ahn, and H. Choudhry: Bioelectrochemistry **143** (2022) 107982. https://doi.org/10.1016/j.bioelechem.2021.107982
54 K. M. Clark, M. S. Schenkel, T. W. Pittman, I. C. Samper, L. B. Anderson, W. Khamcharoen, S. Elmegerhi, R. Perera, W. Siangproh, A. J. Kennan, B. J. Geiss, D. S. Dandy, and C. S. Henry: ACS Meas. Sci. Au **2** (2022) 584. https://doi.org/10.1021/acsmeasuresciau.2c00037
55 I. C. Samper, A. Sánchez-Cano, W. Khamcharoen, I. Jang, W. Siangproh, E. Baldrich, B. J. Geiss, D. S. Dandy, and C.S. Henry: ACS Sens. **6** (2021) 4067. https://doi.org/10.1021/acssensors.1c01527
56 D. Lee, J. Bhardwaj, and J. Jang: Sci. Rep. **12** (2022) 2311. https://doi.org/10.1038/s41598-022-06101-1
57 S. Eissa, K. Al-Kattan, and M. Zourob: ACS Omega **6** (2021) 32072. https://doi.org/10.1021/acsomega.1c04849

58 L. Fabiani, M. Saroglia, G. Galatà, R. De Santis, S. Fillo, V. Luca, G. Faggioni, N. D'Amore, E. Regalbuto, P. Salvatori, G. Terova, D. Moscone, F. Lista, and F. Arduini: Biosens. Bioelectron. **171** (2021) 112686. https://doi.org/10.1016/j.bios.2020.112686

59 J. Zhao, F. Zhao, H. Li, Y. Xiong, S. Cai, C. Wang, Y. Chen, N. Han, and R. Yang: Electrochim. Acta **404** (2022) 139766. https://doi.org/10.1016/j.electacta.2021.139766

60 C. Durmus, S. B. Hanoglu, D. Harmanci, H. Moulahoum, K. Tok, F. Ghorbanizamani, S. Sanli, F. Zihnioglu, S. Evran, C. Cicek, R. Sertoz, B. Arda, T. Goksel, K. Turhan, and S. Timur: Talanta **243** (2022) 123356. https://doi.org/10.1016/j.talanta.2022.123356

61 S. Sanli, F. Ghorbani-Zamani, H. Moulahoum, Z. P. Gumus, H. Coskunol, D. Odaci Demirkol, and S. Timur: Anal. Chem. **92** (2019) 1033. https://doi.org/10.1021/acs.analchem.9b04025

62 Q. Chen: Curr. Opin. Virol. **52** (2022) 148. https://doi.org/10.1016/j.coviro.2021.12.005

63 J. Jaewjaroenwattana, W. Phoolcharoen, E. Pasomsub, P. Teengam, and O. Chailapakul: Talanta **251** (2023) 123783. https://doi.org/10.1016/j.talanta.2022.123783

64 A. G. Ayankojo, R. Borozˇnjak, J. Reut, A. Öpik, and V. Syritski: Sens. Actuators, B **353** (2022) 131160. https://doi.org/10.1016/j.snb.2021.131160

65 S. A. Perdomo, V. Ortega, A. Jaramillo-Botero, N. Mancilla, J. H. Mosquera-DeLaCruz, D. P. Valencia, M. Quimbaya, J. D. Contreras, G. E. Velez, O. A. Loaiza, A. Gomez, and J. de la Roche: IEEE Trans. Instrum. Meas.**70** (2021) 1. https://doi.org/10.1109/TIM.2021.3119147

66 P. K. Sharma, E. S. Kim, S. Mishra, E. Ganbold, R. S. Seong, A. K. Kaushik, and N. Y. Kim: ACS Sens. **6** (2021) 3468. https://doi.org/10.1021/acssensors.1c01437

67 P. H. Chen, C. C. Huang, C. C. Wu, P. H. Chen, A. Tripathi, and Y. L. Wang: Sens. Actuators, B **357** (2022) 131415. https://doi.org/10.1016/j.snb.2022.131415

68 J. Li, R. Lin, Y. Yang, R. Zhao, S. Song, Y. Zhou, J. Shi, L. Wang, H. Song, and R. Hao: ACS Appl. Mater. Interfaces **13** (2021) 22262. https://doi.org/10.1021/acsami.1c05770

69 Y. Chang, Q. Cao, and B. J. Venton: Curr. Opin. Electrochem. **38** (2023) 101228. https://doi.org/10.1016/j.coelec.2023.101228

70 J. S. Stefano, L. R. G. e Silva, R. G. Rocha, L. C. Brazaca, E. M. Richter, R. A. A. Muñoz, and B. C. Janegitz: Anal. Chim. Acta **1191** (2022) 339372. https://doi.org/10.1016/j.aca.2021.339372

71 G. F. Giordano, L. F. Ferreira, Í. R. Bezerra, J. A. Barbosa, J. N. Y. Costa, G. J. C. Pimentel, and R. S. Lima: Anal. Bioanal. Chem. **415** (2023) 3683. https://doi.org/10.1007/s00216-023-04514-z

72 S. Fortunati, C. Giliberti, M. Giannetto, A. Bolchi, D. Ferrari, G. Donofrio, V. Bianchi, A. Boni, I. De Munari, and M. Careri: Biosensors **12** (2022) 426. https://doi.org/10.3390/bios12060426

73 S. Witt, A. Rogien, D. Werner, J. Siegenthaler, R. Lesiyon, N. Kurien, R. Rechenberg, N. Baule, A. Hardy, and M. Becker: Diamond Relat. Mater. **118** (2021) 108542. https://doi.org/10.1016/j.diamond.2021.108542

74 X. Liu, Y. Qiu, D. Jiang, F. Li, Y. Gan, Y. Zhu, Y. Pan, H. Wan, and P. Wang: Microsyst. Nanoeng. **8** (2022) 35. https://doi.org/10.1038/s41378-022-00352-8

75 S. Lin, X. Hu, J. Lin, S. Wang, J. Xu, F. Cai, and J. Lin: Analyst **146** (2021) 4391. https://doi.org/10.1039/D1AN00606A

76 G. Cai, Z. Yu, P. Tong, and D. Tang: Nanoscale **11** (2019) 15659. https://doi.org/10.1039/C9NR05797H

77 K. Takemura, A. B. Ganganboina, I. M. Khoris, A. D. Chowdhury, and E. Y. Park: ACS Sens. **6** (2021) 2605. https://doi.org/10.1021/acssensors.1c00308

78 W. Su, D. Liang, and M. Tan: Trends Food Sci. Technol. **113** (2021) 97. https://doi.org/10.1016/j.tifs.2021.04.053

79 A. Suea-Ngam, L. Bezinge, B. Mateescu, P. D. Howes, A. J. deMello, and D. A. Richards: ACS Sens. **5** (2020) 2701. https://doi.org/10.1021/acssensors.0c01488

80 L. R. Silva, J. S. Stefano, L. O. Orzari, L. C. Brazaca, E. Carrilho, L. H. Marcolino-Junior, M. F. Bergamini, R. A. Munoz, and B. C. Janegitz: Biosensors **12** (2022) 622. https://doi.org/10.3390/bios12080622

81 C. Pina-Coronado, Á. Martínez-Sobrino, L. Gutiérrez-Gálvez, R. Del Caño, E. Martínez-Periñán, D. García-Nieto, M. Rodríguez-Peña, M. Luna, P. Milán-Rois, M. J. S. Castellanos, M. Abreu, R. Cantón, J. G. Galán, T. Pineda, F. Pariente, A. Somoza, T. García-Mendiola, R. Miranda, and E. Lorenzo: Sens. Actuators, B **369** (2022) 132217. https://doi.org/10.1016/j.snb.2022.132217

82 B. Pelaz, V. Grazu, A. Ibarra, C. Magen, P. del Pino, and J. M. de la Fuente: Langmuir **28** (2012) 8965. https://doi.org/10.1021/la204712u

83 K. Kaci, R. Del Caño, M. Luna, P. Milán-Rois, M. Castellanos, M. Abreu, R. Cantón, J. C. Galán, Á. Somoza, R. Miranda, G. González de Rivera, T. García-Mendiola, and E. Lorenzo: Talanta **247** (2022) 123542. https://doi.org/10.1016/j.talanta.2022.123542

84 A. Lomae, P. Preechakasedkit, O. Hanpanich, T. Ozer, C. S. Henry, A. Maruyama, E. Pasomsub, A. Phuphuakrat, S. Rengpipat, T. Vilaivan, O. Chailapakul, N. Ruecha, and N. Ngamrojanavanich: Talanta **253** (2023) 123992. https://doi.org/10.1016/j.talanta.2022.123992

85 T. Vilaivan and C. Srisuwannaket: Org. Lett. **8** (2006) 1897. https://doi.org/10.1021/ol060448q
86 L. Yin, S. Man, S. Ye, G. Liu, and L. Ma: Biosens. Bioelectron. **193** (2021) 113541. https://doi.org/10.1016/j.bios.2021.113541
87 K. Zhang, Z. Fan, Y. Ding, and M. Xie: Chem. Eng. J. **429** (2022) 132472. https://doi.org/10.1016/j.cej.2021.132472
88 L. Wu, X. Wang, C. Wu, X. Cao, T. Tang, H. Huang, and X. Huang: Anal. Chim. Acta **1221** (2022) 340120. https://doi.org/10.1016/j.aca.2022.340120
89 B. Yang, X. Zeng, J. Zhang, J. Kong, and X. Fang: Talanta **249** (2022) 123687. https://doi.org/10.1016/j.talanta.2022.123687
90 C. Wu, Z. Chen, C. Li, Y. Hao, Y. Tang, Y. Yuan, L. Chai, T. Fan, J. Yu, X. Ma, O. A. Al-Hartomy, S. Wageh, A. G. Al-Sehemi, Z. Luo, Y. He, J. Li, Z. Xie, and H. Zang: Nano Micro Lett. **14** (2022) 159. https://doi.org/10.1007/s40820-022-00888-4
91 D. Ji, M. Guo, Y. Wu, W. Liu, S. Luo, X. Wang, H. Kang, Y. Chen, C. Dai, D. Kong, H. Ma, Y. Liu, and D. Wei: J. Am. Chem. Soc. **144** (2022) 13526. https://doi.org/10.1021/jacs.2c02884
92 X. Wang, Z. Hao, T. R. Olsen, W. Zhang, and Q. Lin: Nanoscale **11** (2019) 12573. https://doi.org/10.1039/C9NR02797A
93 H. Zhao, F. Liu, W. Xie, T. C. Zhou, J. OuYang, L. Jin, H. Li, C. Y. Zhao, L. Zhang, J. Wei, Y. P. Zhang, and C. P. Li: Sens. Actuators, B **327** (2021) 128899. https://doi.org/10.1016/j.snb.2020.128899
94 L. Kashefi-Kheyrabadi, H. V. Nguyen, A. Go, C. Baek, N. Jang, J. M. Lee, N. H. Cho, J. Min, and M. H. Lee: Biosens. Bioelectron. **195** (2022) 113649. https://doi.org/10.1016/j.bios.2021.113649
95 Y. Deng, Y. Peng, L. Wang, M. Wang, T. Zhou, L. Xiang, J. Li, J. Yang, and G. Li: Anal. Chim. Acta **1208** (2022) 339846. https://doi.org/10.1016/j.aca.2022.339846
96 Y. Zhang, B. S. Lai, and M. J. Juhas: Molecules **24** (2019) 941. https://doi.org/10.3390/molecules24050941
97 J. F. Wu, X. Gao, L. Ge, G. C. Zhao, and G. F. Wang: RSC Adv. **9** (2019) 19813. https://doi.org/10.1039/c9ra02475a
98 Y. X. Wang, Z.-Z. Ye, C.-Y. Si, and Y.-B. Ying: Chin. J. Anal. Chem. **40** (2012) 634. https://doi.org/10.1016/S1872-2040(11)60542-2
99 S. Ramanathan, S. C. Gopinath, Z. H. Ismail, M. M. Arshad, and P. Poopalan: Biosens. Bioelectron. **197** (2022) 113735. https://doi.org/10.1016/j.bios.2021.113735
100 C. Han, W. Li, Q. Li, W. Xing, H. Luo, H. Ji, X. Fang, Z. Luo, and L. Zhang: Biosens. Bioelectron. **200** (2022) 113922. https://doi.org/10.1016/j.bios.2021.113922
101 Y. J. Yang, Y. Y. Bai, Y. Y. Huangfu, X. Y. Yang, Y. S. Tian, and Z. L. Zhang: Anal. Chem. **94** (2022) 8392. https://doi.org/10.1021/acs.analchem.2c00913
102 G. Kim, J. Kim, S. M. Kim, T. Kato, J. Yoon, S. Noh, E. Y. Park, C. Park, T. Lee, and J. S. Choi: Sens. Actuators, B **352** (2022) 131060. https://doi.org/10.1016/j.snb.2021.131060